Chemical Geology 264 (2009) 43–57

Contents lists available at ScienceDirect

Chemical Geology

journal homepage: www.elsevier.com/locate/chemgeo

High precision SIMS oxygen isotope analysis and the effect of sample topography

Noriko T. Kita *, Takayuki Ushikubo, Bin Fu [1], John W. Valley

WiscSIMS Laboratory, Department of Geology and Geophysics, University of Wisconsin–Madison, 1215 W. Dayton St., Madison, WI 53706, USA

ARTICLE INFO

Article history:
Received 5 November 2008
Received in revised form 12 February 2009
Accepted 15 February 2009

Editor: R.L. Rudnick

Keywords:
Secondary ion mass spectrometer
Isotope ratios
Oxygen
High precision
Instrumental bias

ABSTRACT

We have developed highly precise and accurate *in situ* SIMS stable isotope analytical protocols using the IMS-1280 at the University of Wisconsin, through careful tuning of the instrument, stable electronics, and improved protocols for sample preparation, standardization and automated analysis. Multicollection Faraday Cup (FC) oxygen two and three isotope analyses routinely achieve spot-to-spot reproducibility of 0.3‰ ($\delta^{18}O$ and $\delta^{17}O$, 2SD) from 10–15 μm single spots. Accuracy can be even better for multiple analyses of a homogeneous sample. Furthermore, reproducibility at the ≤1‰ level is achieved by using multi-collection FC–Electron Multiplier (EM) analyses for primary ion beam spots of 1 to 3 μm in diameter. These results present a trade-off vs. conventional laser fluorination techniques; sample sizes are 10^6 to 10^9 times smaller, at the expense of a factor of 2 to 10 in analytical precision. SIMS is now a powerful tool for high precision and accuracy, *and* high spatial resolution stable isotope studies and provides the potential for fundamental new advances in stable isotope geochemistry.

Analytical artifacts from sample geometry and topography (X–Y effects) are examined in detail. Several epoxy mounts containing mineral standards were prepared and the amounts of polishing relief were measured using an optical profilometer. No significant X–Y effect is identified within 7 mm from the center of the mount when the grains are polished flat with minimal relief (≤1 μm). However, significantly large topographic effects are found from standard grains with relatively large polishing relief (10–40 μm). The measured values of $\delta^{18}O$ vary depending on the amount of relief, inclination of surface, and geometry of analytical spots on the standard grains, resulting in elevated $\delta^{18}O$ value by as much as ~4‰ and degraded external precision as poor as ±3‰ (2SD). These analytical artifacts may be caused by deformation of the local electrostatic field applied on the surface of the sample, which deviates the trajectory of secondary ions of individual isotopes. The results clearly indicate that polishing relief for highly accurate SIMS stable isotope analyses should be less than a few μm, which can be readily evaluated by using an optical surface profilometer.

1. Introduction

The secondary ion mass spectrometer (SIMS, or ion microprobe) has been used to examine isotopic ratios and trace element abundance of geological samples at 20–30 μm-scale (e.g., Shimizu et al., 1978; Ireland, 1995; Valley et al., 1998). For oxygen isotope analyses, SIMS has been used to detect micro-distribution of oxygen isotope ratios with permil (‰)-level precision in terrestrial samples (Valley and Graham, 1991) and mass-independent ^{16}O enrichments in meteoritic samples (e.g., McKeegan et al., 1998; Yurimoto et al., 1998). However, application of SIMS to stable isotope analyses has been relatively limited due to insufficient precision and accuracy to resolve sub-‰ level natural variations seen in geological samples. Precision and accuracy are partly limited by the total number of secondary ions produced by the limited analytical volume (typically 20–30 μm diameter with ~μm depth). It is also limited by the poor reproducibility of repeated analyses of standard, which may be related to both the condition of samples as well as stability of the instrument. Furthermore, the instrumental bias of the measured isotope ratio may depend strongly on the matrix and considerable effort is required to obtain matching standards with homogeneous isotope ratios for accurate corrections.

Recently, multicollection Faraday Cup (FC) detectors on IMS-1270 instruments have been applied for high precision sub-permil SIMS isotope analyses (Schumacher et al., 2004), including oxygen two isotope ($^{18}O/^{16}O$) and three isotope ($^{18}O/^{16}O$ and $^{17}O/^{16}O$) measurements (e.g., Gurenko et al., 2001; Kita et al., 2004; Cavosie et al., 2005; Nemchin et al., 2006a,b; Treble et al., 2005, 2007; Whitehouse and Nemchin, 2009). More recently, Ickert et al. (2008) also demonstrated sub‰ precision oxygen isotope analysis technique using SHRIMP II, another large-radius ion microprobe that has been mainly used for geochronology. However, some of these earlier multi-detector studies encountered difficulty in obtaining consistently reproducible and accurate results, even though the internal precision of single analyses was better than 0.5‰ (2SD; standard deviation).

* Corresponding author. Tel.: +1 608 233 7118; fax: +1 608 262 0693.
E-mail address: noriko@geology.wisc.edu (N.T. Kita).
[1] Present address: School of Earth Sciences, The University of Melbourne, Parkville, VIC 3010, Australia.

0009-2541/$ – see front matter © 2009 Elsevier B.V. All rights reserved.
doi:10.1016/j.chemgeo.2009.02.012

We have achieved significant success in obtaining ≤0.3‰ (2SD) level precision and accuracy for oxygen isotope ratio measurement by using a new generation large radius secondary ion mass spectrometer, IMS-1280, installed in 2005 at the WiscSIMS laboratory, University of Wisconsin – Madison (Fig. 1). This instrument has been used for a wide range of stable isotope geochemistry and cosmochemistry investigations (Desbois et al., 2007; Eiler et al., 2007; Kelly et al., 2007; Weidel et al., 2007; Bindeman et al., 2008; Downes et al., 2008; Moser et al., 2008; Ushikubo et al., 2008; Wilde et al., 2008; Bowman et al., 2009; Lancaster et al., 2009; Orland et al., 2009). In addition, there could be many samples having several ‰ variations within a 10 μm-scale domain that could not be studied using 10–30 μm spot sizes of previous generation SIMS. For such fine-scale projects, we developed 1–3 μm small beam analyses with moderate precision (≤1‰; Page et al., 2007; Nakamura et al., 2008; Kozdon et al., 2009). In this paper, we report the analytical developments to achieve sub ‰ precision routinely. We also address reproducibility and accuracy of oxygen isotope measurements. During the course of these studies, we realized the importance of the flatness of the samples for reproducible results. For this reason, we performed systematic tests on standards with various amounts of polishing relief and evaluate the effect of relief on precision and accuracy.

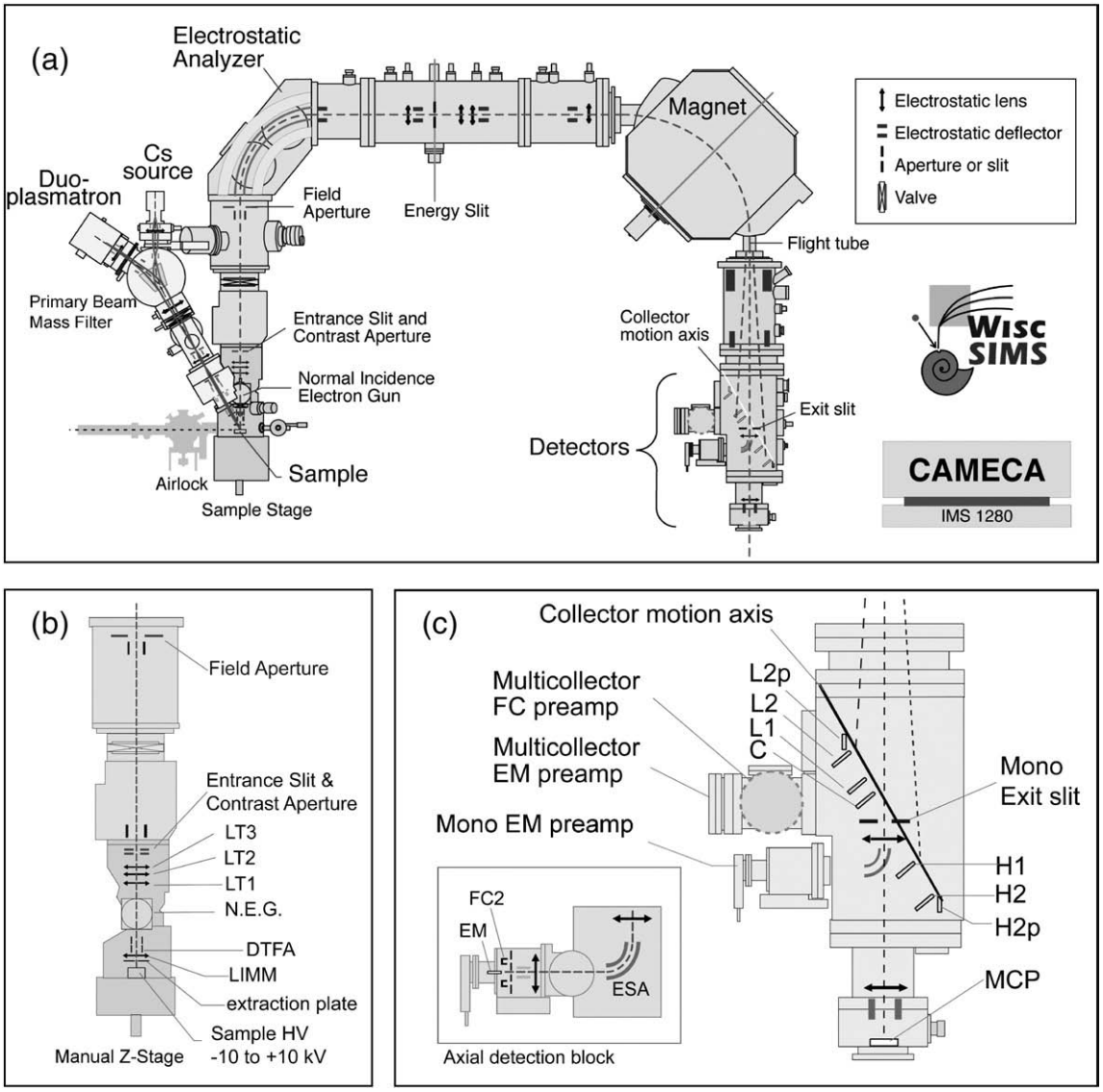

Fig. 1. A schematic diagram of the IMS-1280. (a) Overview. The IMS-1280 is a double focusing mass spectrometer equipped with two primary ion sources (Cs source and Duoplasmatron source for oxygen primary ions). In geochemical applications, Cs^+ and O^- primary ions induce more negative secondary ions (e.g., C^-, O^-, Si^-, S^-) and positive secondary ions (e.g., Li^+, Mg^+), respectively. Primary ions are deflected by the primary beam mass filter into the primary beam column. A Normal Incidence Electron Gun (NEG) is used for charge compensation in Cs^+ primary and negative secondary mode. Secondary ion optics of the IMS-1280 consist of three parts; transfer optics from sample (±10 kV) to the Field Aperture (FA), coupling optics from the electrostatic analyzer (ESA) to the sector magnet, and projection optics including 10 ion detectors. (b) Secondary ion transfer optics of the IMS-1280. The secondary accelerating voltage (±10 kV) is applied to sample surface. The sample stage height is manually adjusted by *Z*-focusing stage. Secondary ions produced on the sample surface are projected to the Field Aperture (FA) located at the entrance of ESA. The magnification of ion image from sample to FA is determined by the choice of three transfer lenses (LT1, LT2, LT3). DTFA is a set of deflectors (*X* and *Y*) that are used for automatic centering of the secondary ions to the FA (see text for more detail). An electron beam is emitted with accelerating voltage of −10 kV from the NEG locating above the transfer optics, deflected by a magnetic coil along the ion optical axis, and exposed to sample surface where electrons lose energy because of equipotential applied to NEG and secondary ion accelerated voltages. (c) Detection system of the IMS-1280. The IMS-1280 is equipped 10 ion detectors; 2 Faraday Cups (FC) and 1 Electron multiplier (EM) on the axial detection system (or "Mono collection system") and 4 FCs and 3 small EM on multicollection system. A multi-channel plate (MCP) is located at the end of ion axis for direct ion imaging. The Mono collection system uses the adjustable width exit slit (Mono exit slit) and an ESA to deflect secondary ions to detectors. Multicollection detectors are on trolleys moving along the collector motion axis, which approximate the focal plane of the secondary ions. The Mono collection exit slit and projection lens (between Mono exit slit and ESA) are lifted and the ESA is swung out from the multicollection motion axis when multi-collection detectors should move to a position close to the center. The Mono collection system can be used together with multicollection system for applications such as C isotopes, oxygen three isotopes, Si and S two isotope ($^{30}Si/^{28}Si$ and $^{34}S/^{32}S$), in which ^{13}C, ^{17}O, ^{30}Si and ^{34}S are on the Mono collection detector, respectively.

2. Conditions of SIMS oxygen isotope analysis

2.1. High precision oxygen two isotope analyses using multicollection FC mode

In Table 1, we summarize the oxygen two isotope analytical conditions using ~10 μm Cs^+ primary beam, the electron gun and multicollection Faraday Cup detectors. One of the main differences from previous studies using IMS-1270 is the significantly higher sensitivity of oxygen secondary ions from a 10 μm spot ($^{16}O \sim 3\times10^9$ cps; $\sim10^9$ cps/nA of primary beam current) because of both higher primary ion intensity (2–3 nA) and high secondary ion transmission (~90%; compared to the condition with slits and apertures fully opened). The high secondary ion transmission is achieved by the transfer lens optics of 200 times magnification using a combination of two transfer lenses (LT2 and LT3 in Fig. 1b) closer to contrast aperture and entrance slit position (Kita et al., 2004), which is difficult to tune because of the higher level of aberration on the mass spectrum. The useful yield, as defined by the ratio of the number of secondary ions detected and the number of atoms sputtered, is estimated to be ~7% for the case of UWG-2 garnet standard (Supplementary data A1). Under our analytical conditions, consumption of the sample in our SIMS analyses is typically ≤1 ng for ~10 μm spots and as small as 1–2 pg with the sub-1 μm spot size (Page et al., 2007).

We use a focused Cs^+ primary ion beam ("Gaussian beam") in order to obtain much higher primary beam density than in "Kohler illumination" mode. Due to the short analysis time (~3.5 min, Table 1), the depth of SIMS pit is very shallow (≤1 μm) compared to its diameter (10–15 μm). Although the Kohler illumination mode, which creates a flat-bottomed pit, has been considered to be superior to irregular dish shaped pit in obtaining reproducible results (McKeegan et al., 1998; Kita et al., 2004), a focused primary beam in our analytical protocol does not create significant topographic effects and the analysis results are not affected.

Table 1
Analytical condition of SIMS oxygen two isotope measurements at WiscSIMS.

Primary ions	Focused Cs^+ ions, 2.5 nA and 10 μm diameter. Accelerated by +10 kV	
Electron-gun for charge compensation.	Accelerated by −10 kV with sample current 30 μA. Homogeneous across 60 μm × 100 μm oval area.	
Secondary HV	Accelerated by −10 kV at the sample surface. (Total primary ion acceleration to sample surface is 20 kV)	
Transfer optics	Magnification of ×200 from sample to Field Aperture (4 mm × 4 mm)	
Entrance slit	120 μm width	
Contrast aperture	400 μm diameter	
Energy slit	40 eV width, the inner edge is adjusted at the position 5 eV lower than the peak of energy distribution with 5 eV window.	
Exit slit	500 μm	
Mass resolving power	~2200 (10% height)	
Secondary ion intensities	$^{16}O = 3\times10^9$cps	$^{18}O = 6\times10^6$cps
Detector and amplifier	Multi FC (10^{10} ohm)	Multi FC (10^{11} ohm)
Detector noise	<10,000 cps for 4 s integration	<3,000 cps for 4 s integration
Relative transmission through mass spectrometer	~90% (full transmission is defined as apertures and slit fully opened)	
Magnetic field control	NMR (Nuclear Magnetic Resonance) with magnetic field stability ≤5 ppm over 10 h. Recalibrate every 12 h.	
Centering of secondary ions	Manual *Z*-focusing and automatic adjustment of secondary deflectors	
FC base line measurement	64 s integration once a day	
Integration time	80 s (4 s × 20 cycles)	
Total analysis time per spot	3.5 min including presputtering (10 s) and automated re-centering (2 min)	
Internal precision	≤0.2‰ for $^{18}O/^{16}O$ (2SE)	
External (spot-to-spot) precision	≤0.3‰ for $^{18}O/^{16}O$ (2SD)	

In order to achieve high reproducibility, the beam of the electron gun is carefully tuned at the beginning of each session in terms of electron current applied to the surface of the sample (~30 μA on Al/Cu-mesh with 20 V offset), centering to the secondary ion optics, and homogeneity (60 μm × 100 μm oval area, which is observed using ^1H image induced by electron beam from surface correlated hydrogen on the sample). The magnetic field is maintained stable within 10 ppm (or 5ppm in mass) by using a NMR (Nuclear Magnetic Resonance) probe and readjusted every 12 h. The primary beam trajectory is at ~21° angle against normal to the sample surface (deflected from 30°), so that any slight height difference along the sample surface is identified as a shift of primary beam position. In each analysis position, sample height is manually adjusted (*Z*-focus) to minimize the shift of primary beam position (less than 10 μm on the sample surface), which is supposed to reproduce the height of the sample stage within ~30 μm against the secondary ion extraction plate (5 mm away from the sample surface). Furthermore, there is a slight deformation of the electrostatic field applied to the sample surface (−10 kV) towards to edge of the 1-inch (~25 mm) holder, which can cause deflection of secondary ions away from the ion optical center. These effects are minimized by automated centering of the secondary ion beam in the field aperture prior to each analysis using deflectors near the first cross over of the secondary ions.

Each analysis takes about 3.5 min, consisting of 10 s of presputtering, ~120 s of automated centering of secondary ions, and 80 s of integrating oxygen isotope signals. Because of high primary beam density, 10 s presputtering is long enough to achieve nearly full strength of the secondary oxygen ion intensity, which is subsequently stabilized during the 120 s period of automated centering prior to integrating the ion counts. Under the analytical conditions described above with typical count rates of $\sim3\times10^9$ cps and $\sim6\times10^6$ cps for $^{16}O^-$ and $^{18}O^-$, respectively, the internal precision from one spot analysis consisting of 20 cycles (80 s total integration) of oxygen two isotope measurements ($^{18}O/^{16}O$ ratio) is typically ~0.2‰ (2SE; SE = standard error), which is consistent with the thermal noise of the Faraday Cup amplifiers (~2000 cps for 4 s integration in 1SD).

2.2. Oxygen three isotope analyses and small spot (≤3 μm) analyses

We further expand our analytical capabilities to oxygen three isotope analyses using three FC detectors (for 10–15 μm spots) and oxygen two (or three) isotope analyses with small beam spots (≤3 μm) using FC-EM (electron multiplier) detectors. A similar condition described above is applied, except for choice of detectors, mass resolving power (as defined by entrance and exit slit widths) and analysis time.

For the oxygen three isotope analyses, ^{17}O is measured using an axial detector with mass resolution of ~5000 (at 10% height) in order to resolve the OH interference. The axial detector (also called "Mono collection system" as it is not on the multicollection trolley) is equipped with a variable width exit slit and the ^{17}O beam can be deflected either on FC or EM depending on the ^{17}O intensities. We typically use the FC for intensities greater than 5×10^5 cps and the EM for intensities lower than $\sim3\times10^5$ cps. The entrance slit is set to 75 μm and the exit slit at the axial detector is adjusted to ~200 μm, while keeping the largest exit slit widths (500 μm; MRP~2000) for ^{16}O and ^{18}O on the multicollection as in the case of the oxygen two isotope analyses. The transmission of the secondary ions decreases to ~70% because of the narrower entrance slit width compared to the oxygen two isotope analysis condition. The contribution of $^{16}O^1H$ interference to the ^{17}O signal is estimated by obtaining the relative intensity of the ^{17}O mass spectrum at 0.0036 amu below ^{17}O (equivalent to the mass difference between $^{16}O^1H$ and ^{17}O), which determines the shape of the tailing correction. The relative intensity is always kept less than 20 ppm. Here we assume that the shapes of the mass spectrum of ^{17}O and $^{16}O^1H$ are the same, which should be applied with caution. We consider this to be good approximation in

our analytical condition because the direct ion image of $^{16}O^{1}H$ is very similar to that of ^{17}O. Multiplying the relative sensitivity by ($^{16}O^{1}H/^{17}O$) ratios gives the hydride correction factor, which is usually negligible for anhydrous materials (<0.1‰ for $^{16}O^{1}H/^{17}O$ ratios less than 5). By using ~15 μm beam with a primary ion intensity of 4–5 nA, which is higher than the above oxygen two isotope analysis, a single spot analysis takes ~8 min for multicollection FC oxygen three isotope measurements. In this condition, the internal errors of $^{17}O/^{16}O$ and $^{18}O/^{16}O$ ratios are typically 0.3 and 0.1‰ (2SE), respectively, from 40 cycles (total 400 s) of measurements.

For the small spot analyses, the primary ion beam is finely focused typically to ≤3 μm diameter with a low primary Cs^{+} intensity of ≤20 pA. The minimum diameter of the primary beam for oxygen isotope analysis is 0.9×0.6 μm with Cs+ intensity of 1 pA and secondary ^{16}O intensity of 10^{6} cps (Page et al., 2007). The secondary ion intensities of minor oxygen isotopes (^{17}O and ^{18}O) are less than 10^{5} cps, so that they are measured using EM detectors in pulse counting mode. The ^{17}O beam is put on a large ETP EM in the axial position, while a small EM detector (Hamamatsu) on the multicollection trolley is used for ^{18}O. The EM pulse heights are adjusted to have a peak at ~280 mV at the beginning of each analysis session. The gain of EM detector does not drift significantly if the count rates are less than 10^{5} cps, though readjustments are required a few to several times a day unless the count rates are much less than 10^{4} cps. A single spot analysis takes between 15 and 30 min for small spot analyses depending on the beam size; time is inversely related to the count rate of the minor isotope to collect total counts of at least 4×10^{6} (i.e., statistical error of 1‰ in 2SD). A presputtering time is required between 3 and 10 min at the beginning of each analysis in order to stabilize the secondary ion intensity, which is much longer than 10 s for a larger primary ion beam of the multicollection FC analyses. During the presputtering, the base line of the FC detector for ^{16}O is measured in each analysis, otherwise the baseline drift could be as large as ~1000 cps within a day and bias the measured oxygen isotope ratios (both $^{18}O/^{16}O$ and $^{17}O/^{16}O$) as much as 1‰.

2.3. Reproducibility of the mineral standards

In the above section, internal errors of a single analysis were described for different analytical conditions. However, it is important to emphasize that internal precision is not a good index of analysis quality for stable isotope ratios by SIMS. It is often the case that actual spot-to-spot reproducibility on a homogeneous standard is significantly worse than internal precision. In other cases, isotope ratios systematically change within a single analysis so that the external precision of repeated analyses is better than the internal precisions. We demonstrate here various test analyses using homogeneous oxygen isotope standards in order to evaluate external (spot-to-spot) reproducibility of oxygen isotope analyses.

Through this paper, the raw measured ($^{18}O/^{16}O$) ratios are converted to delta notation $\delta^{18}O_{RAW}$, by normalizing to Standard Mean Ocean Water $(^{18}O/^{16}O)_{VSMOW}=0.0020520$, (Baertschi, 1976). Since the absolute ($^{17}O/^{16}O$) ratio of VSMOW is not known with high precision, the normalization parameter $(^{17}O/^{16}O)=0.000383$ is used to convert the measured ratio to $\delta^{17}O_{RAW}$, in agreement with the estimate of $(^{17}O/^{16}O)_{VSMOW}=0.0003831$ by McKeegan (1987). The $\delta^{18}O$ values on the VSMOW scale that were calibrated by conventional extraction techniques and gas-source mass spectrometer are expressed as "$\delta^{18}O$" throughout the paper.

2.3.1. Reproducibility as a function of sample stage position

In order to test the reproducibility of oxygen isotope ratio measurements across the sample surface, we analyzed small fragments of a zircon standard with homogeneous oxygen isotope ratios (KIM-5,

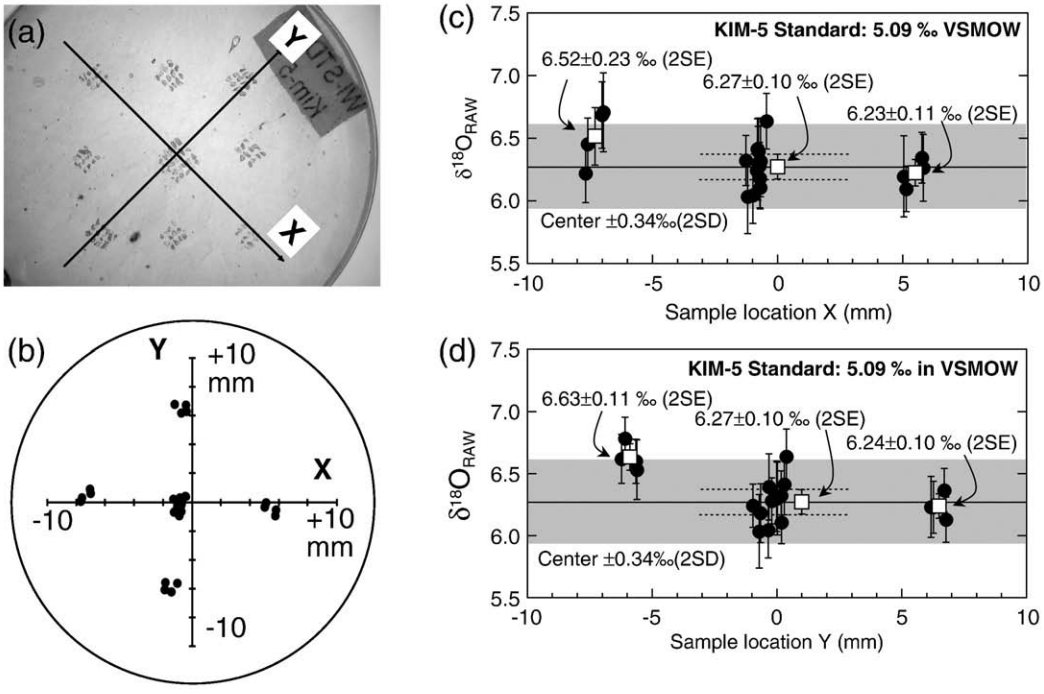

Fig. 2. Reproducibility of SIMS analyses of $\delta^{18}O$ for zircon standard, KIM-5, as a function of non-optimum sample geometry (uncorrected raw data, grain mount WI-STD-12). (a) Reflected light image of the mount before gold coating, showing 9 groups of zircon standard grains cast in epoxy resin as a grid with a ~5 mm interval. The mount was inserted to the instrument rotated as shown in Fig. 2b to perform a test at *X* and *Y* coordinates of ±7 mm. (b) Map of analysis spots on the mount. Units are mm. The outer circle indicates the edge of the epoxy mount, 25 mm diameter. The stage *X* and *Y* coordinates correspond to the sample surface. (c, d) Variation of $\delta^{18}O_{RAW}$ values along the stage *X*-*Y* coordinates. Data are listed in Table A2. The solid line and grey regions are the average and the external (spot-to-spot) reproducibility (2SD) of 12 analyses from the group of grains near the mount's center (6.27 ± 0.34‰), which is slightly better than that of all the analyses, 6.35 ± 0.42‰ (2SD, $N=28$). The average and standard errors (in 2SE) of multiple analyses are shown from five locations as open squares. Although individual $\delta^{18}O_{RAW}$ values from extreme locations (*X* or *Y* >5 mm) overlap with those from near the center, the average of four analyses at $Y=-6$ mm (6.63 ± 0.11‰, 2SE) is significantly higher than that of 12 analysis near the center (6.27 ± 0.10‰, 2SE), with difference of 0.36 ± 0.14‰ (2SE).

$\delta^{18}O = 5.09‰$ VSMOW, Valley, 2003; Page et al., 2007). We used the conditions for oxygen two isotope analyses in multicollection FC mode and the results are shown in Fig. 2. In this mount (WI-STD-12, Fig. 2a), more than 100 small chips of the original KIM-5 crystal are cast within the central 7 mm radius of a 25 mm round epoxy resin mount in order to simulate typical geological samples prepared for SIMS analyses (such as zircon U–Pb geochronology mounts). The zircon grains are polished flat against the epoxy surface showing minimal polishing relief (≤0.5 μm) as determined by profilometer measurements. The reproducibility of analyses at the center of the mount is 0.34‰ (2SD), whereas pits that are 6–7 mm from the center show a marginal variation depending on location within the mount. The largest deviation in Fig. 2 is observed at $Y = -6$ mm with the average $\delta^{18}O_{RAW}$ value $0.36 \pm 0.14‰$ higher than at the center of the mount (Fig. 2d). Such geometrical effects are here called "X–Y effects". In the case of the zircon standard mount with a well polished, flat surface, the effect within 6–7 mm from the center is marginal and comparative to the reproducibility of the repeated analyses at the central location.

2.3.2. Reproducibility within an analysis session

The above protocol for oxygen two isotope analysis in multicollection FC mode allows us to obtain more than 300 spot analyses in a day (24 h). Fig. 3 demonstrates an example of reproducibility of UWQ-1 quartz standard ($\delta^{18}O = 12.33‰$ VSMOW; Kelly et al., 2007) mounted in multiple samples and measured in a continuous 48 h analysis session (Rusk et al., 2007). All the UWQ-1 standard grains were mounted within 5 mm of the center of each mount. The average and external precision of $\delta^{18}O_{RAW}$ of 173 analyses of UWQ-1 is $6.75 \pm 0.42‰$ (2SD) among a total of 658 spot analyses within 48 h. Although we changed sample mounts 11 times during the session, there is no significant change in UWQ-1 data before and after a sample change. The UWQ-1 data in Fig. 3a demonstrate small, but consistent amounts of drift of ~0.2‰ over 48 h (except for the last sample change), which is the level equivalent to small drift of FC noise of ~1000 cps.

Because of potential minor drift or in some cases a sudden change, 4 spots analyses of UWQ-1 are made every 15–20 analyses as a monitor. The analyses of unknown samples are corrected for instrumental bias calculated from the average of 8 bracketing standard analyses using the method described later in 2.4. The reproducibility (external precision) of each set of 8 bracketing standard analyses is assigned as the analytical uncertainty of each single spot analysis within that bracket. In the session shown in Fig. 3, the average of external precision is 0.29‰ (2SD), which is slightly worse than the typical internal error of the analysis (~0.2‰ in 2SE).

In most cases, internal precision of a single analysis is comparable to or smaller than the external spot-to-spot precision on standards. However, for some minerals including calcite and albite, we consistently attain smaller external precision (≤0.3‰) than internal precision (~0.5‰). For these minerals, the measured isotope ratio varies systematically with depth during a single analysis. However, high reproducibility for single analyses is achieved due to constant analysis depth with a given primary beam condition and a carefully timed analysis routine. While many minerals do not yield changes in measured ratio at such shallow depths, depth profiling analysis is not advisable without testing a homogeneous standard.

The reproducibility of oxygen three isotope analyses (Kita et al., 2008) is shown in Fig. 4 to demonstrate the performance of multicollection FC mode with 15 μm diameter spots. San Carlos olivine grains (SC; $\delta^{18}O = 5.32‰$ VSMOW, Kita et al., 2007) were mounted around the edge of meteorite sections within ~5 mm of the center of the mounts. Three grains from the first mount and one from the second mount are analyzed as bracketing standards. The average external precisions of $\delta^{18}O_{RAW}$ and $\delta^{17}O_{RAW}$ values from 8 sets of bracketing analyses are 0.31‰ and 0.37‰ (2SD), respectively. The external reproducibility of $\delta^{18}O_{RAW}$ is significantly worse than that of internal precision (0.1‰, 2SE). Yet, the external precision of ~0.3‰ is similar to minor X–Y effects seen in Fig. 2.

The reproducibility of oxygen two isotope measurements from a small beam analysis using multicollection FC-EM mode is shown in Fig. 5. In this example, several foram samples were analyzed with UWC-3 calcite as bracketing standard ($\delta^{18}O = 12.49‰$ VSMOW; Kozdon et al., 2009). Before the third analysis of every set of four standards, the gain of the EM detector was adjusted slightly by

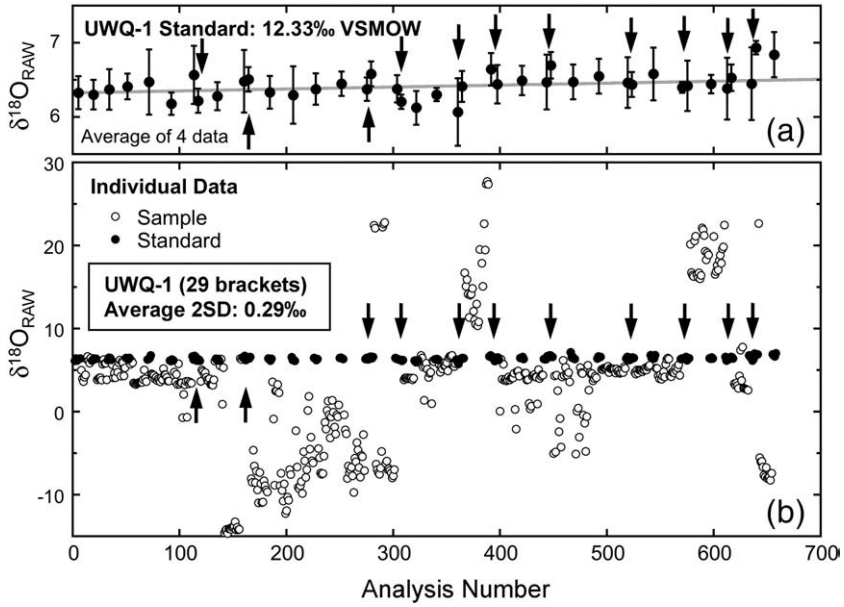

Fig. 3. Optimized reproducibility SIMS analyses of $\delta^{18}O$ of multiple grains of quartz standard (UWQ-1) in 12 sample mounts with quartz unknowns during one analysis session (uncorrected raw data, Rusk et al., 2007). A total of 658 analyses were made within 48 h including 173 standard analyses; standard analyses were made in groups of four spot analyses. (a) The average and 2SD of each group of 4 standard analyses. There is a small amount of drift with time shown as grey line (~0.2‰/48 h). The arrows indicate sample changes. The $\delta^{18}O_{RAW}$ values in standard quartz grains in different sample mounts indicate that the sample change does not generally affect the measured ratios. (b) All data from the 48 h session. The external errors of sample analyses are estimated by the 2SD of 8 analyses from the two groups of bracketing standards for each group of 10–20 sample analyses. The average value of 2SD of 8 analyses in a standard bracket is better than 0.3‰. The standard quartz analyses (filled symbols) are constant while values from natural and synthetic quartz samples (open circles) vary by 40‰.

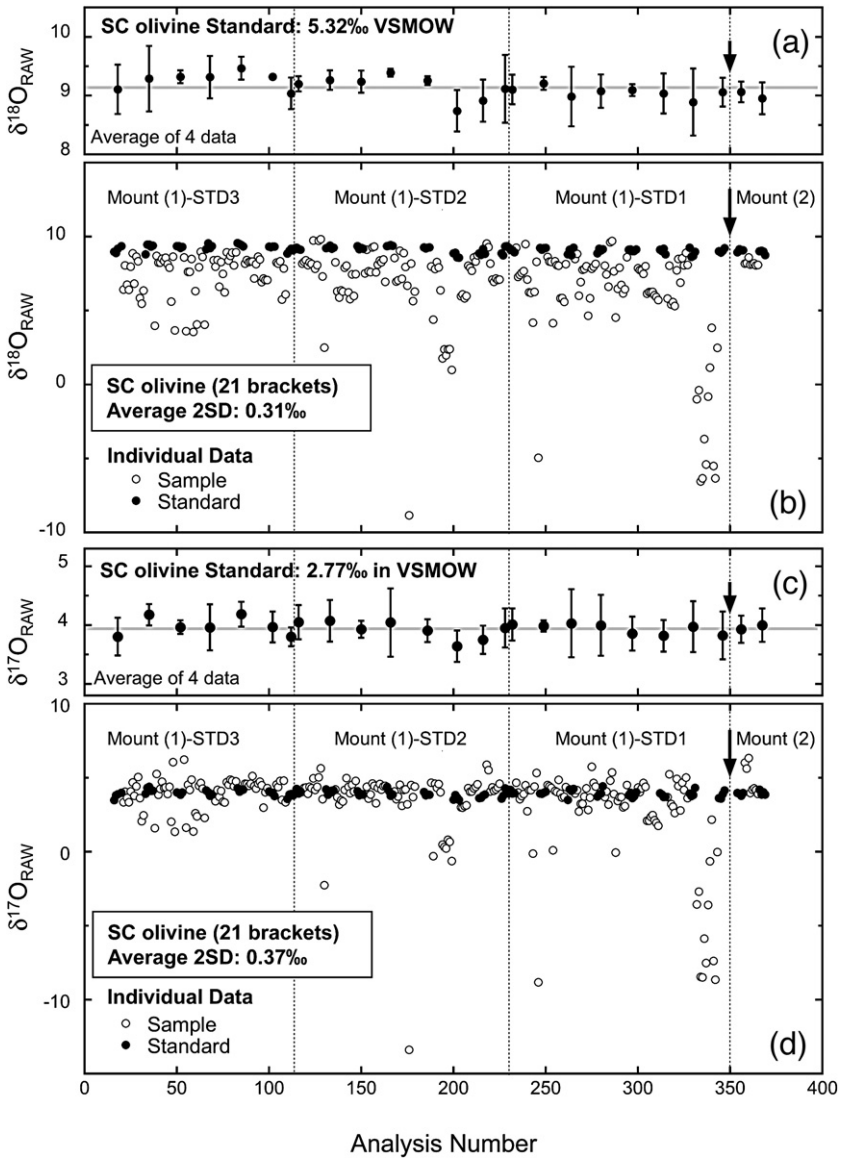

Fig. 4. Optimized reproducibility of San Carlos olivine standard (SC) for SIMS oxygen three isotope analyses in multicollection FC mode during meteorite sample analysis sessions (uncorrected raw data, Kita et al., 2008). A total of 343 analyses were made within 56 h including 103 standard analyses. (a) Average $\delta^{18}O_{RAW}$ and 2SD values of each group of standard analyses (4 analyses/group). (b) The $\delta^{18}O_{RAW}$ values of all analyses during the session. (c) Average $\delta^{17}O_{RAW}$ and 2SD values of each group of standard analyses (4 analyses/group). (d) The $\delta^{17}O_{RAW}$ values of all analyses. Filled symbols are SC standard and open symbols are meteorite analyses. Two thick sections of meteorite specimens, Mounts (1) and (2) were analyzed. Arrows indicate sample change to Mount (2). In Mount (1), three SC standards (STD1, STD2, STD3) are placed around the edge of the meteorite specimen, with the *X* and *Y* coordinates (in mm) of (+1.0, +3.3), (−4.5, +1.1), (0.5, −5.1), respectively. No significant difference among them in measured ratios was observed. The averages of 2SD of bracketing standard analyses (total 8 analyses before and after sample analyses) are 0.31‰ and 0.37‰ for the $\delta^{18}O_{RAW}$ and $\delta^{17}O_{RAW}$ values, respectively. The error bars in (a) and (c) are 2SD of each group of four standard analyses.

increasing EM high voltage (~ a few volts). Without this adjustment, the UWC-3 data would show systematic drift through the analysis session due to aging of the EM. The external precisions of bracketing standard analyses are 0.7‰ (2SD) on average, which is significantly larger than the internal precision of ~0.4‰ (2SE) mainly from counting statistics. There could be a source of additional error, though it is difficult to evaluate a small effect comparable to the internal precision. One possibility is a small drift of EM gain (~0.5‰) during 9 sets of analyses while keeping the EM high voltage constant. Total dose of ^{18}O ions detected by the EM during 10 analyses is $\sim 3\times10^8$ counts, which may be large enough to cause the observed minor drift.

2.4. Instrumental bias correction

The SIMS measured isotope ratios are subjected to instrumental bias (often called Instrumental Mass Fractionation) according to the differences in the ionization efficiency of individual isotope, in the transmission through the mass spectrometer and efficiency of individual detectors. Therefore, the measured ratios are always biased compared to the true value and a correction is necessary to convert to the VSMOW scale. Standards with homogeneous oxygen isotope ratios and calibrated $\delta^{18}O$ values are used during each analysis session to correct the instrumental bias. The SIMS instrumental bias is known to include large matrix effects and thus standards should usually be the same mineral phase as the sample and have similar chemical composition. For minerals with complex solid solution or zoning such as carbonates or garnets, it may be required to have many standards so that the instrumental bias can be interpolated from a suite of standards with chemical composition bracketing that of the unknowns (Eiler et al., 1997a,b; Vielzeuf et al., 2005). The matrix specific SIMS instrumental bias correction is often referred as “matrix correction”. More general procedures for the SIMS matrix corrections have been described (Hervig

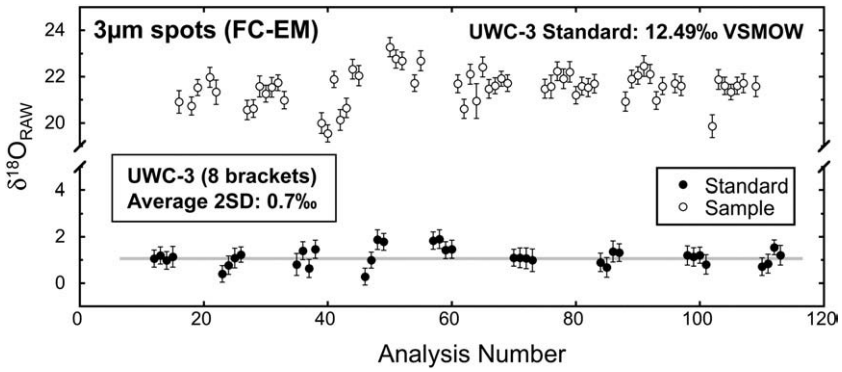

Fig. 5. Optimized reproducibility of SIMS analyses of $\delta^{18}O$ for UWC-3 calcite standard during a session with a 3 μm diameter primary beam spot (uncorrected raw data). Data are from Kozdon et al. (2009) who report oxygen isotope zoning in single foram tests. The oxygen isotope analyses were performed using multicollection FC-EM mode. The primary Cs^+ and secondary $^{16}O^-$ ion intensities were ~20pA and 2×10^7 cps, respectively. The integration time was 800 s. A total of 94 analyses were made within 48 h including 36 standard analyses. Filled symbols are UWC-3 analyses and open symbols are analyses of foram samples. The EM high voltage was adjusted before the third of four standard analyses. The average of 2SD of bracketing standard analyses is 0.7‰, while the average internal precision is ~0.4‰ (2SE), which is consistent with the counting statistics (i.e., total $\sim3\times10^7$ counts of ^{18}O in a single analysis).

et al., 1992; Eiler et al., 1997a; Riciputi et al., 1998), but no other procedure provides accuracy at sub-permil levels.

We define $\alpha^{18}O_{SIMS}$ as follows to describe the instrumental bias of the measured value (SIMS) vs. the value on the VSMOW scale.

$$\alpha^{18}O_{SIMS} = \frac{1 + \left(\delta^{18}O_{RAW} / 1000\right)}{1 + \left(\delta^{18}O / 1000\right)} \tag{2.1}$$

Because $\alpha^{18}O_{SIMS}$ is often very close to unity, it is useful to define the instrumental bias in permil deviation of $\alpha^{18}O_{SIMS}$ from the unity;

$$\alpha^{18}O_{SIMS} = [1 + (\text{bias} / 1000)] \tag{2.2}$$

The logarithms of Eqs. (2.1) and (2.2) result in the following formula;

$$ln[1 + (\text{bias} / 1000)] = ln\left[1 + \left(\delta^{18}O_{RAW} / 1000\right)\right] - ln\left[1 + \left(\delta^{18}O / 1000\right)\right] \tag{2.3}$$

If the instrumental bias, $\delta^{18}O_{RAW}$, and $\delta^{18}O$ are all smaller than ±10‰, then Eq. (2.3) leads to the approximation in Eq. (2.4), which is accurate within 0.1‰;

$$(\text{bias}) \approx \delta^{18}O_{RAW} - \delta^{18}O \tag{2.4}$$

For example, the UWQ-1 quartz standard ($\delta^{18}O = 12.33$‰ VSMOW) analyses in Fig. 3 show an average $\delta^{18}O_{RAW}$ of 6.80‰, which gives nearly identical bias values of −5.47‰ and −5.53‰ by using Eqs. (2.3) and (2.4), respectively. The approximation in Eq. (2.4) is often applicable to the oxygen isotope analyses of geologic samples and has been frequently used in SIMS studies. However, there are many natural samples with a wide variation of $\delta^{18}O$. Some minerals and/or analytical procedures would produce large instrumental bias. Therefore, Eq. (2.4) should only be applied to studies with sub-permil precisions if $\delta^{18}O$ values are sufficiently close to unity (O'Neil, 1986, Table 1). It is especially important to evaluate this approximation with other isotope systems, such as H or S, where natural fractionations greater than 10‰ can be common. Therefore, we calibrate instrumental bias from bracketing standards using $\alpha^{18}O_{SIMS}$-notation (in Eq. (2.1)) without approximation and obtain isotope ratios of unknown samples on the VSMOW scale.

$$\delta^{18}O = \left\{\left[1 + \left(\delta^{18}O_{RAW} / 1000\right)\right] / \alpha^{18}O_{SIMS} - 1\right\} \times 1000 \tag{2.5}$$

The instrumental bias during an analysis session is estimated from the analyses of the isotope standard that bracket unknown sample analyses. The examples of standard analyses shown in Figs. 2–5 correspond to the instrumental bias of zircon, quartz, olivine and calcite to be +1.2‰, −5.8‰, +3.8‰ and −11‰, respectively. The instrumental bias on calcite in FC-EM mode (−11‰) is more negative than in FC-FC mode (−3.2‰) for the same standard reported by Orland et al. (2009), which is due to the lower detection efficiency of EM compared to FC by nearly 1%. More normally, using the same detectors and analysis protocol, the instrumental biases of individual minerals vary by at most 1–2‰ from session to session. However, the instrumental bias will change from instrument to instrument as well as depending on the analytical conditions and detector settings. The fairly small session-to-session variations in bias that we observe is in part due to reproducible analytical setting and measurement protocols as described in this paper.

The instrumental biases of the SIMS oxygen isotope analyses observed in this study do not show the large negative values that were obtained from some studies in the past (as much as −80‰; e.g., Hervig et al., 1992; Eiler et al., 1997a; Leshin et al., 1997). These studies with large negative bias used energy filtering with significant reduction of secondary ion transmission compared to this work. In contrast, bias values from more recent literature without energy offset do not show large negative values (e.g., Gurenko et al., 2001; Kita et al., 2004; Cavosie et al., 2005; Nemchin et al., 2006a; Kelly et al., 2007; Treble et al., 2007; Ickert et al., 2008). For C and Si isotope analyses performed in the WiscSIMS laboratory using the analytical conditions similar to that of oxygen isotope analyses, we do see a large negative instrumental bias (<−30‰); $\delta^{13}C$ from carbonate and diamond (Weidel et al., 2007; Liu et al., 2008) and $\delta^{30}Si$ from silicates (Knight et al., in press). It is interesting to note that the secondary ion productions of C and Si from these minerals are 10–100 times lower than that of oxygen in the same analytical condition. Therefore, it is possible that preference of light isotope enrichment created by sputtering induced ionization is related to ionization efficiency and the effect is small for oxygen isotope due to relatively high ionization efficiency.

For oxygen three isotope analyses, the instrumental mass fractionation for ($^{17}O/^{16}O$) ratio is defined as $\alpha^{17}O_{SIMS}$ similar to the case of ($^{18}O/^{16}O$) ratio.

$$\alpha^{17}O_{SIMS} = \frac{1 + \left(\delta^{17}O_{RAW} / 1000\right)}{1 + \left(\delta^{17}O / 1000\right)} \tag{2.6}$$

It should be noted that $\delta^{17}O$ values of standards are calculated from $\delta^{18}O$ values by using an exponential mass fractionation law with a β factor of

0.52; $[1+(\delta^{17}O/1000)]=[1+(\delta^{18}O/1000)]^{0.52}$ (Clayton et al., 1991), because the standards are natural terrestrial minerals and we usually calibrate $\delta^{18}O$ values from the conventional gas-source mass spectrometry that does not independently measure $\delta^{17}O$.

It is evident from the above description of instrumental bias correction and error assignments that the final accuracy and precision of the SIMS stable isotope analyses depend on the quality of isotope standards. If the oxygen isotope ratios of standard minerals are heterogeneous at the scale of SIMS analysis, then instrumental bias corrections based on conventional fluorination analyses of bulk materials will not be accurate. Evaluating the homogeneity of standards is a major hurdle for any *in situ* technique. If even a small portion of the standard differs from the rest, this will not be a concern for bulk analysis where many grains are analyzed together, however serious systematic errors could result for *in situ* analyses calibrated against a single grain.

The mineral standards used at WiscSIMS are extensively tested for homogeneity prior to use as an isotope standard for microanalysis and calibration during analysis is typically based on more than one grain. In order to evaluate potential standard materials, we crush candidate samples to small fragments (<500 μm) and randomly select chips or grains for both laser fluorination and SIMS analyses. As a first step, sample homogeneity can be evaluated at the mm-scale with precision better than 0.2‰ (2SD) by analyzing many mg-sized chips by laser fluorination (Valley et al., 1995). These analyses also provide a calibration of oxygen isotope ratios on the VSMOW scale. If the mg-sized samples are homogeneous in $\delta^{18}O$, we further perform SIMS analyses to examine homogeneity among grains and to evaluate a larger portion of the standard material. It is common to examine many samples before one is found to be satisfactory as a standard. More detailed discussion about instrumental bias correction method from various minerals and solid solutions are presented elsewhere (e.g., Eiler et al., 2007; Kita et al., 2007; Ushikubo et al., 2008; Kozdon et al., 2009).

3. Effect of sample relief on the $\delta^{18}O_{RAW}$ using SIMS

The secondary ions created from the sample surface by sputtering with a Cs^+ primary ion beam are first accelerated by 10 kV, the potential difference between sample surface (−10 kV) and the extraction plate 5 mm above the sample. Geologic samples are often electrically insulating phases mounted in epoxy resin that must be coated with thin conductive layers (typically ~30 nm C or Au) for charge neutralization. Any surface topography of the sample (or standard) will deform the equipotential surfaces parallel to the sample surface, which may deform the path of secondary ion trajectory and affect the measured isotope ratios. Sample relief can have many causes. During the grinding and polishing of samples, polishing relief is often created, especially during the final <1 μm grit process. This is a particular problem among minerals with different hardness or at the boundary of grains surrounded by epoxy. Relief can also be created in epoxy by electron beam instruments used to image samples in grain mounts; this can generally be avoided with careful attention and low sample currents. Analysis of the rims of mineral grains is often of interest, especially to investigate diffusion profiles, interaction between solid and melt (and/or fluid), or growth of different generations of minerals. Because of the high precision achieved at WiscSIMS, permil-level effects from isotope diffusion and various isotope reservoirs can be clearly resolved or ruled out (Desbois et al., 2007; Kelly et al., 2007; Page et al., 2007; Kozdon et al., 2009). However, surface topography of the sample could produce false results if not properly controlled, for example values could be biased by polishing relief at the edge of a grain mimicking a diffusion profile.

In order to evaluate the level of analytical artifacts, we conducted three experiments: (1) the effect of polishing relief by intentionally varying the amounts of relief from <1 μm to 40 μm on zircon standard grain mounts and (2) the effect of polishing relief at the boundary of one grain of a homogeneous quartz standard. In these experiments, we used a ZYGO™ white light profilometer at the Materials Science Center,

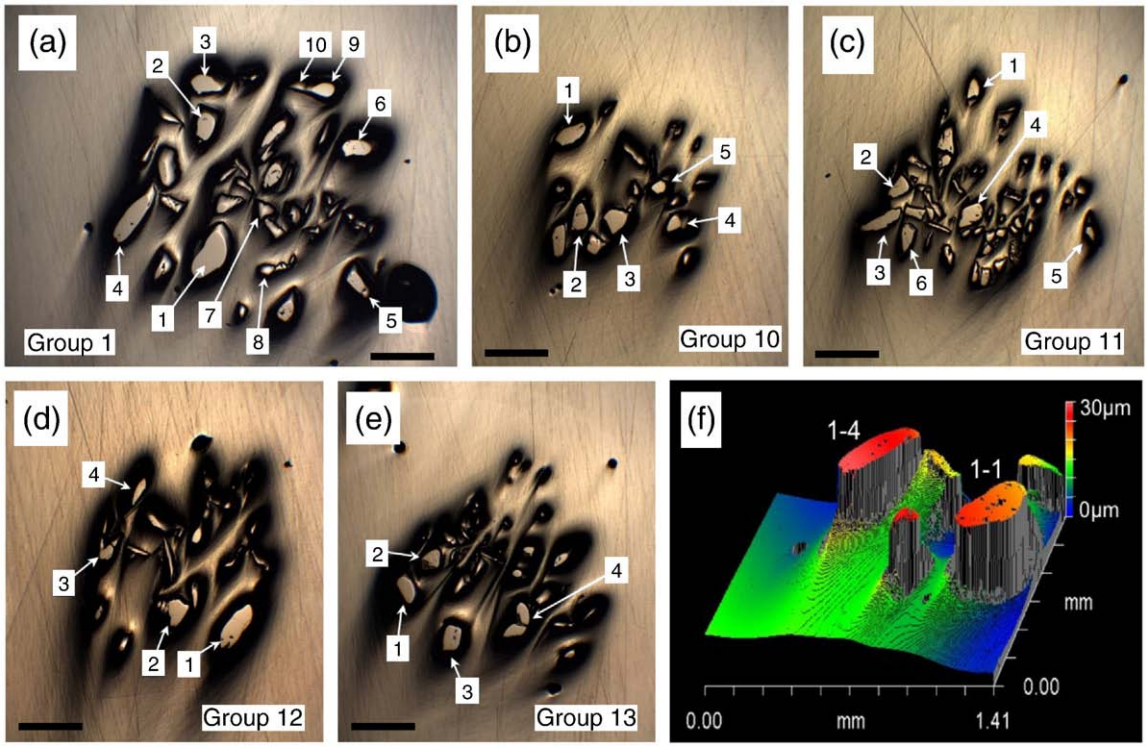

Fig. 6. Not optimized standard zircon grains (KIM-5) in WI-STD-13 after the first step of polishing (Step-1). (a–e) Reflected light images of Groups 1, 10, 11, 12 and 13. Grains that are labeled with numbers are those for oxygen isotope analyses. Scale bars, 0.5 mm. (f) Polishing relief measured by using the profilometer for the lower left of Group 1. Field of view — 1.4 × 1.0 mm. The maximum polishing relief in this area is 30 μm. Two large grains marked as 1-1 and 1-4 are those shown in (a). Epoxy at the left side of the grain 1-4 is lower (blue) that at other locations (green).

University of Wisconsin–Madison to measure surface topography at the sub-μm scale. (3) In comparison to these tests of non-ideal sample preparation, we also performed the third experiment by analyzing the rim of a diopside standard grain with a minimum of relief (<1 μm).

3.1. Intentionally applied polishing relief on zircon standard (KIM-5)

We used the polished grain mount, WI-STD-13, which contains ~200 chips of zircon standard (KIM-5) and is similar to WI-STD-12 shown in Fig. 2. The 200 to 500 μm diameter grains of zircon in WI-STD-13 are mounted as 13 groups of 10–20 grains/each within 7 mm of the center of the mount. Both of these zircon mounts were originally prepared with minimal relief (<1 μm) and repeated analyses of randomly selected grains show reproducibility of $\delta^{18}O_{RAW}$ of 0.3‰ (2SD, as shown in Fig. 2).

3.1.1. Creation of variable polishing relief

Step-1: The mount, WI-STD-13, was re-polished with 0.3 μm alumina powder with high-nap pad on a quickly rotating lap in order to erode the epoxy and create polishing relief. After the sample was ultrasonically cleaned with water, we applied 1 min of repolishing using 3 μm diamond lapping film by hand to partially flatten the top of the high relief grains, but not to remove all relief. The 0.5 μm diamond lapping film was used subsequently to remove scratches made in 3 μm polishing. Some grains still had rounded surface because alumina powder polishing created a variety of heights

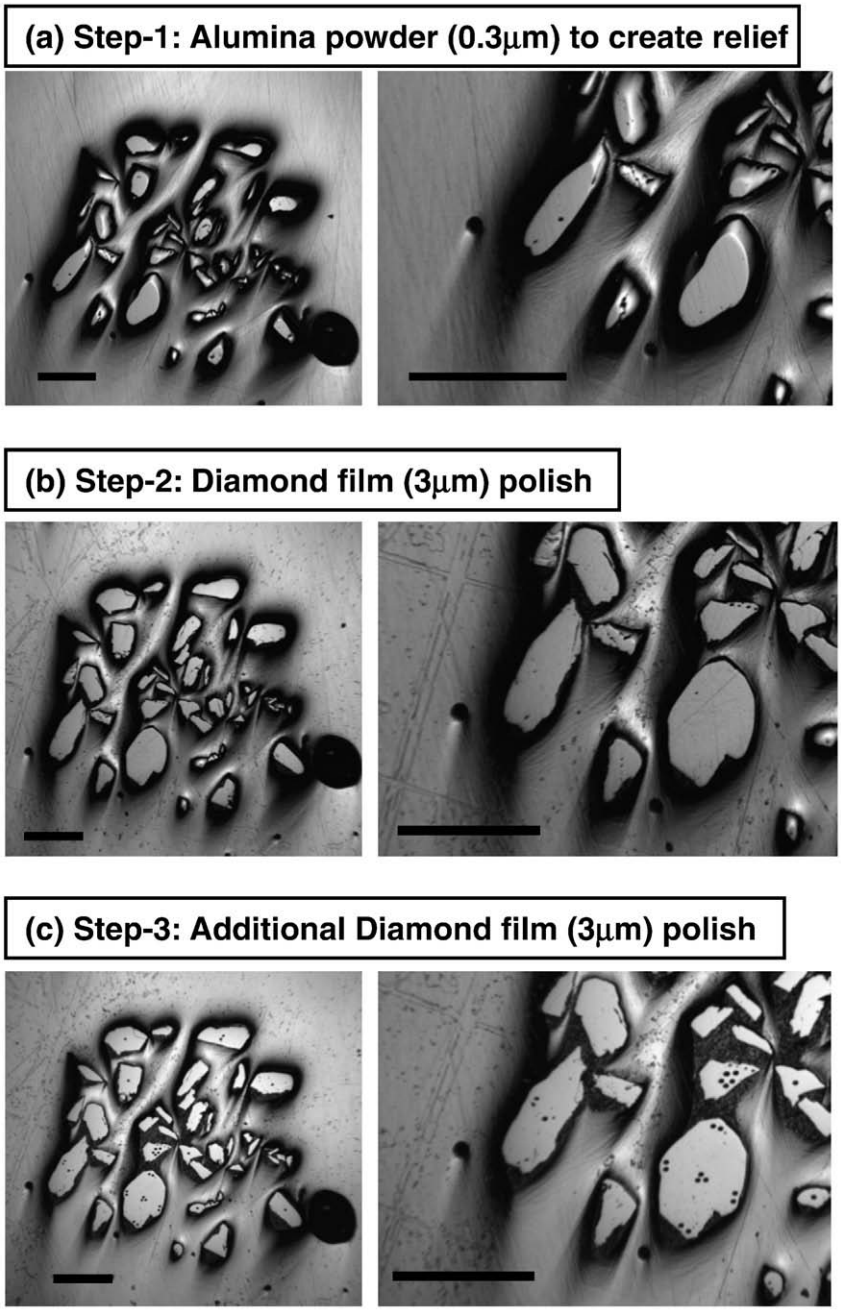

Fig. 7. Reflected light images of zircons after three polishing steps from Group 1 at the center of the mount WI-STD-13 (Fig. 6a). (a) Step-1, (b) Step-2 and (c) Step-3. See text for detailed polishing process. Scale bars are 0.5 mm. The average amounts of relief in the region were 29 μm, 22 μm and 20 μm for Step-1, -2, -3, respectively. The images in (c) are taken after the SIMS analyses, showing pits on the center of the grains (the left side image). In contrast, one large grain in the lower right image (Group-1 grain "1"; also shown again in Fig. 10) shows many pits made to evaluate the effect of analyzing near the rim of a grain.

among grains. The surface topography of a group of zircon grains against the epoxy resin was measured by using the profilometer. The relief of five groups on the mount (group names, 1, 10, 11, 12, and 13; Fig. 6a–e) ranged from 22 μm to 40 μm, defined as maximum height difference between grain surface and immediately adjacent epoxy resin. In each group, epoxy resin at periphery of the group of grains was eroded deeper than epoxy between the grains, causing the zircon grains to rise above a "plateau". There are streamlined troughs in epoxy on both sides of each group of zircons (partly seen in Fig. 6f) with the same orientation throughout the section. These troughs were made during the alumina powder polishing because we did not rotate the epoxy mount.

*Steps-2 and -3: M*ount WI-STD-13 was gently ground down using a 3 μm diamond film in two additional steps to reduce the amount of relief (Steps-2 and 3). A 0.5 μm diamond lapping film was used subsequently to remove scratches made in 3 μm polishing. Profilometer measurements were performed for three groups for the Step-2 (groups 1, 10 and 12) and only one group for the Step-3 (group 1), indicating that the sample was ground down ~5 μm at each step, though relief was not fully removed even after the Step-3. The reflected light images of the same grains for three steps are compared in Fig. 7. After the first polishing step, many grains still show a rounded surface, which is fully flattened in the second step. However, all the grains are well above the surface of the epoxy resin. After the last step, the amount of relief was variable from 0 to 25 μm; in places the epoxy surface became level with the zircon grains and started to polish.

3.1.2. SIMS analyses of multiple grains

The SIMS measurements were made for randomly selected grains from five groups for Step-1, three groups for Step-2 and only one group for Step-3, from which profilometer measurements were performed. The results of analyses ($\delta^{18}O_{RAW}$) are shown in Table 2. The topography of each group measured using profilometer is also shown in Table 2. We intentionally analyzed the center of each grain in order to avoid additional effects at the edge of high relief grains that could also be significant. For Step-1, a second standard mount with grains of the same zircon (KIM-5) and low relief (WI-STD-12), was measured before and after the analyses for comparison and as a monitor of potential instrumental drift. The results of Step-1 are shown in Fig. 8, showing the average and 2SD of 28 spot analyses to be 7.7 ± 1.8‰. This is biased and poorly reproducible compared to zircons on mount WI-STD-12 (an average of 6.7 ± 0.3‰ in 2SD). The average $\delta^{18}O_{RAW}$ values and the 2SD from five different groups of zircon grains were variable, ranging from 7.3‰ to 8.8‰ for $\delta^{18}O_{RAW}$ and the precision (2SD) varies from 0.7‰ to 2.6‰ (Table 2). Among grains in each group, the grain at lowest *X* coordinates (right side of Fig. 6a–e) always shows highest $\delta^{18}O_{RAW}$ values. The large variation of $\delta^{18}O_{RAW}$ values along *X* coordinates may be related to the surface topography of individual groups that are more pronounced in the direction parallel to the polishing troughs on the epoxy resin (Fig. 6f).

For Steps-2 and -3, we did not measure WI-STD-12 in the same session and only the reproducibility of analyses was evaluated, which range from ±0.6‰ to 1.5‰ (2SD). As shown in Fig. 9 summarizing all data from the three grinding steps, the external precisions of $\delta^{18}O_{RAW}$ values generally correlate with the amounts of relief. The grains from Group 1 of the mount were analyzed in all three steps, showing an improvement of external precision (2SD) with the polishing steps. These results clearly indicate that external precision of $\delta^{18}O_{RAW}$ improves with reduction of the amount of polishing relief.

3.1.3. SIMS analyses of a single grain

In addition to the above analyses at the center of multiple grains, we selected one large zircon grain from mount WI-STD-13 (Group 1, grain "1" in Fig. 6a and f) and analyzed both the center and the rim of the

Table 2
SIMS raw oxygen isotope ratios ($\delta^{18}O_{RAW}$) of KIM-5 zircon standard grains ($\delta^{18}O$ = 5.09‰ VSMOW) measured with variable amounts of polishing relief.

Analysis#	Position[a]	$\delta^{18}O_{RAW}$	error	*X* mm	*Y* mm	Relief[b] (μm)
Mount Name: WI-STD-12 KIM-5 bracket for Step-1						
S1-08	1-1	6.71	0.22	0.9	−0.6	
S1-09	1-2	6.68	0.24	−0.2	−0.3	
S1-10	1-3	7.05	0.28	1.0	1.0	
S1-11	1-4	6.90	0.19	1.3	−0.7	
S1-62	1-5	6.65	0.32	−0.4	0.6	
S1-63	1-6	6.77	0.26	−0.2	−0.4	
S1-64	1-7	6.58	0.20	1.3	−0.6	
S1-65	1-8	6.74	0.25	1.1	1.0	
Average and 2SD (*N* = 8)		**6.76**	**0.30**			**<0.5**
Mount Name: WI-STD-13 (Step-1)						
S1-30	1-2	7.7	0.2	−0.6	−0.1	
S1-31	1-3	8.3	0.3	−0.7	0.2	
S1-32	1-4	8.5	0.3	−1.1	−0.9	
S1-33	1-5	6.6	0.2	0.7	−1.2	
S1-34	1-6	6.5	0.3	0.6	−0.2	
S1-35	1-7	8.1	0.2	−0.1	−0.8	
S1-36	1-8	7.1	0.2	−0.1	−1.2	
S1-37	1-9	6.7	0.3	0.3	0.3	
S1-38	1-10	7.5	0.3	0.1	0.3	
Average and 2SD		**7.4**	**1.5**			**29**
S1-39	10-1	7.7	0.3	−6.9	−0.5	
S1-40	10-2	7.9	0.3	−6.7	−1.2	
S1-41	10-3	7.6	0.4	−6.5	−1.2	
S1-42	10-4	7.6	0.3	−6.0	−1.1	
S1-43	10-5	6.9	0.5	−6.1	−0.9	
Average and 2SD		**7.5**	**0.7**			**24**
S1-44	11-1	6.6	0.3	−0.3	6.9	
S1-45	11-2	7.8	0.3	−0.8	6.1	
S1-46	11-3	8.3	0.4	−1.0	5.8	
S1-47	11-4	7.1	0.3	−0.2	5.9	
S1-48	11-5	6.5	0.2	0.7	5.9	
S1-49	11-6	7.3	0.3	−0.7	5.7	
Average and 2SD		**7.3**	**1.3**			**22**
S1-50	12-1	7.5	0.3	6.9	−0.5	
S1-51	12-2	8.1	0.3	6.5	−0.4	
S1-52	12-3	9.1	0.4	5.9	0.0	
S1-53	12-4	7.4	0.3	6.1	0.5	
Average and 2SD		**8.0**	**1.6**			**40**
S1-54	13-1	10.4	0.4	−0.7	−6.8	
S1-55	13-2	9.0	0.3	−0.5	−6.6	
S1-56	13-3	8.7	0.3	−0.3	−7.2	
S1-57	13-4	7.3	0.4	0.2	−7.0	
Average and 2SD		**8.8**	**2.6**			**35**
Average and 2SD of WI-STD-13 (*N* = 28)		**7.7**	**1.8**			
Single grain (1-1) center and rim						
S1-24	1-1-#1	7.7	0.3	−0.52	−1.12	
S1-25	1-1-#2	8.5	0.2	−0.62	−1.26	
S1-26	1-1-#3	7.5	0.2	−0.48	−0.96	
S1-27	1-1-#4	8.0	0.3	−0.57	−1.10	
S1-28	1-1-#5	6.5	0.3	−0.41	−1.13	
S1-29	1-1-#6	7.2	0.3	−0.48	−1.11	
S1-66	1-1-#7	7.6	0.2	−0.55	−1.15	
S1-67	1-1-#8	4.1	0.4	−0.39	−1.12	
S1-68	1-1-#9	9.0	0.3	−0.65	−1.07	
S1-69	1-1-#10	7.1	0.2	−0.48	−0.88	
S1-70	1-1-#11	7.2	0.3	−0.59	−1.30	
Average and 2SD		**7.3**	**2.5**			**21**
WI-STD-13 (Step-2)						
S2-50	1-4	7.1	0.3	−1.1	−0.6	
S2-51	1-5	6.1	0.3	0.3	−0.7	
S2-52	1-6	6.0	0.3	0.3	0.7	
S2-53	1-9	6.3	0.2	−0.1	1.0	
S2-54	1-3	6.8	0.2	−1.0	0.6	
S2-55	1-2	6.7	0.3	−0.9	0.3	
S2-56	1-7	6.3	0.2	−0.2	−0.1	
Average and 2SD		**6.5**	**0.8**			**22**
S2-57	10-1	7.5	0.3	−6.5	−2.4	
S2-58	10-2	6.8	0.2	−6.1	−2.9	
S2-59	10-3	6.8	0.2	−5.9	−2.8	

Table 2 (*continued*)

Analysis#	Position[a]	$\delta^{18}O_{RAW}$	error	*X* mm	*Y* mm	Relief[b] (μm)
WI-STD-13 (Step-2)						
Average and 2SD						
S2-60	10-4	6.9	0.2	−5.5	−2.6	
S2-61	10-5	7.0	0.3	−5.7	−2.4	
Average and 2SD		**7.0**	**0.6**			**19**
S2-62	12-1	6.3	0.2	6.3	2.7	
S2-63	12-2	6.7	0.2	5.9	2.6	
S2-64	12-3	7.9	0.3	5.1	2.8	
S2-65	12-4	7.0	0.2	5.2	3.4	
Average and 2SD		**7.0**	**1.4**			**34**
Single grain (1-1) center and rim						
S2-44	1-1-#1	6.5	0.2	−0.38	−0.62	
S2-45	1-1-#2	6.2	0.3	−0.39	−0.39	
S2-46	1-1-#3	5.6	0.3	−0.24	−0.56	
S2-47	1-1-#4	7.7	0.2	−0.41	−0.81	
S2-48	1-1-#5	6.8	0.1	−0.52	−0.61	
S2-49	1-1-#6	6.2	0.2	−0.33	−0.61	
Average and 2SD		**6.5**	**1.5**			**15**
WI-STD-13 (Step-3)						
S3-15	1-8	6.1	0.3	0.0	−0.4	
S3-16	1-5	5.5	0.4	0.7	−0.4	
S3-17	1-7	6.2	0.3	−0.1	0.1	
S3-18	1-6	5.9	0.4	0.7	0.6	
S3-19	1-9	5.9	0.4	0.3	1.1	
S3-20	1-3	6.5	0.4	−0.5	1.1	
S3-21	1-2	6.0	0.3	−0.5	0.8	
S3-22	1-4	6.2	0.3	−1.1	0.0	
Average and 2SD		**6.0**	**0.6**			**20**
Single grain (1-1) center and rim						
S3-4	1-1-#1	6.0	0.2	−0.48	−0.24	
S3-5	1-1-#2	6.1	0.3	−0.41	−0.05	
S3-6	1-1-#3	6.0	0.4	−0.62	−0.21	
S3-7	1-1-#4	6.6	0.3	−0.54	−0.47	
S3-8	1-1-#5	5.8	0.4	−0.35	−0.36	
S3-9	1-1-#6	5.7	0.4	−0.49	−0.26	
S3-10	1-1-#7	6.0	0.3	−0.38	−0.06	
S3-11	1-1-#8	6.3	0.3	−0.61	−0.18	
S3-12	1-1-#9	6.5	0.3	−0.57	−0.44	
S3-13	1-1-#10	5.9	0.3	−0.34	−0.32	
S3-14	1-1-#11	5.7	0.3	−0.46	−0.26	
Average and 2SD		**6.1**	**0.6**			**10**

[a] For WI-STD-13, names of positions are defined as "group number – grain number". For the multiple analyses of the single grain (grain 1-1), additional numbers "-#n" indicate the sequence of analysis.

[b] The relief of zircon grains against epoxy surface is determined using profilometer.

grain. Profilometer measurements indicate that surface topography around this grain was reduced from ~21 μm to ~10 μm for the three polishing steps. The results are shown in Table 2 and Fig. 10. The $\delta^{18}O_{RAW}$ values deviate significantly at the rim, showing external precisions of 2.5‰ and 1.5‰ (2SD) for Steps-1 and -2, respectively. These external precisions are much worse than that obtained by analyzing the centers of multiple grains in the same group; 1.5‰ and 0.8‰ for Steps-1 and -2, respectively. The reproducibility is improved for Step-3, showing precision of 0.6‰ (2SD) and identical to the analyses of multiple grains. These results indicate that analytical artifacts due to sample topography are emphasized at the edge of grains compared to the center.

There is also a systematic variation of the $\delta^{18}O_{RAW}$ values that correlates to *X*–*Y* coordinates; increasing $\delta^{18}O_{RAW}$ values with decreasing *X* and *Y* coordinates. Smaller *X* coordinates (spots #4 and #9 in Step-1, #5 in Step-2, and #3 and #8 in Step-3, in Fig. 10) always shows higher values than opposite locations (spots #5 and #8 in Step-1, #3 in Step-2 and #5 and #10 in Step-3, in Fig. 10). Smaller *Y* coordinates (spots #2 in Step-1, #4 in Step-2, and #4 and #9 in Step-3, in Fig. 10) always show higher values than opposite locations (spots #3 in Step-1, #2 in Step-2 and #2 and #7 in Step-3, in Fig. 10). In particular, data from near the rim on sloped surfaces (#8 and #9 in Step-1, in Fig. 10) show over a 5‰ difference.

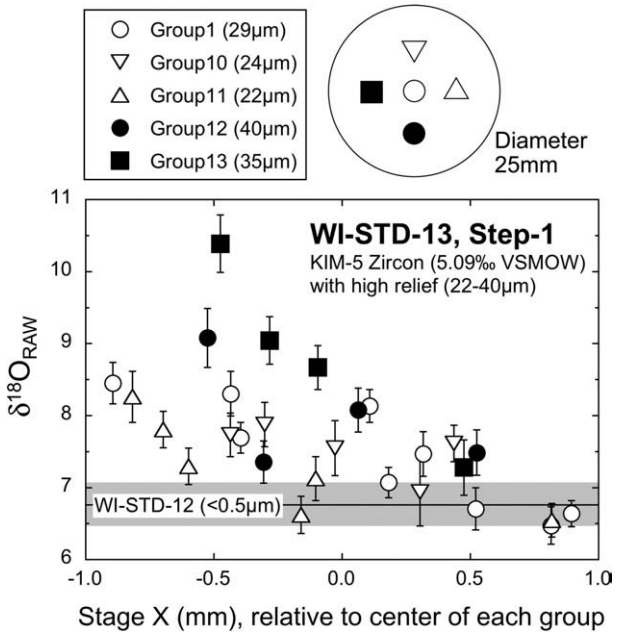

Fig. 8. SIMS oxygen isotope analyses of standard zircon grains (KIM-5) with relief of 22–40 μm (Step-1). Data from five groups (1, 10, 11, 12 and 13) of zircon grains on WI-STD-13 (Fig. 6) are shown with different symbols. Data are shown in Table 2. The location of each group on the mount is tabulated as *X*–*Y* coordinates in Table 2 and shown in the map (lower right). The horizontal axis is *X* coordinate relative to the center of each group. Shadowed area indicates the reproducibility of KIM-5 grains from a different mount with minimal relief (WI-STD-12, $\delta^{18}O_{RAW} = 6.7 \pm 0.3$‰ in 2SD), measured in the same session (Table 2), while the average of 28 spots in 5 groups on WI-STD-13 ($\delta^{18}O_{RAW} = 7.7 \pm 1.8$‰) is relatively elevated. In all groups, data with lower or more negative *X* coordinates are systematically higher in $\delta^{18}O_{RAW}$. This tendency is emphasized for data from higher relief grains (groups 12 and 13).

3.2. Polishing relief on quartz standard (UWQ-1)

Mount WI-STD-8 contains more than 50 grains of the quartz standard, UWQ-1, and had a moderate amount of polishing relief, typically ~10 μm as measured by profilometer. We chose one large grain (~1.5 mm dia.) showing up to 12 μm relief between epoxy and the grain surface (Fig. 11a, b), and measured oxygen isotope ratios from the rim and center of the grain. The results are shown in Fig. 11c.

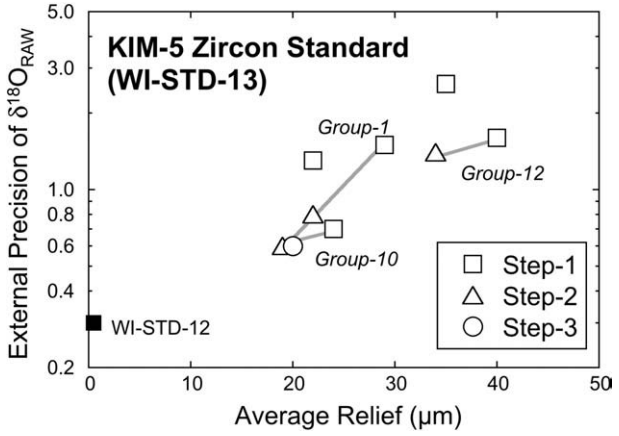

Fig. 9. External precision (2SD) of SIMS oxygen isotope analyses ($\delta^{18}O_{RAW}$) of KIM-5 zircon standard grains with variable amounts of polishing relief. Data are shown in Table 2. The reproducibility of analyses is shown on the *Y*-axis as a logarithmic scale. Each data point corresponds to one group of zircon grains from polishing Steps-1, -2 and -3. Open symbols are from WI-STD-13; squares are Step-1, triangles are Step-2 and a circle is Step-3. A filled symbol is from WI-STD-12 with minimal relief (≤0.5 μm) during the same session with Step-1. Data from the same group improve in external precision with reduction of polishing relief.

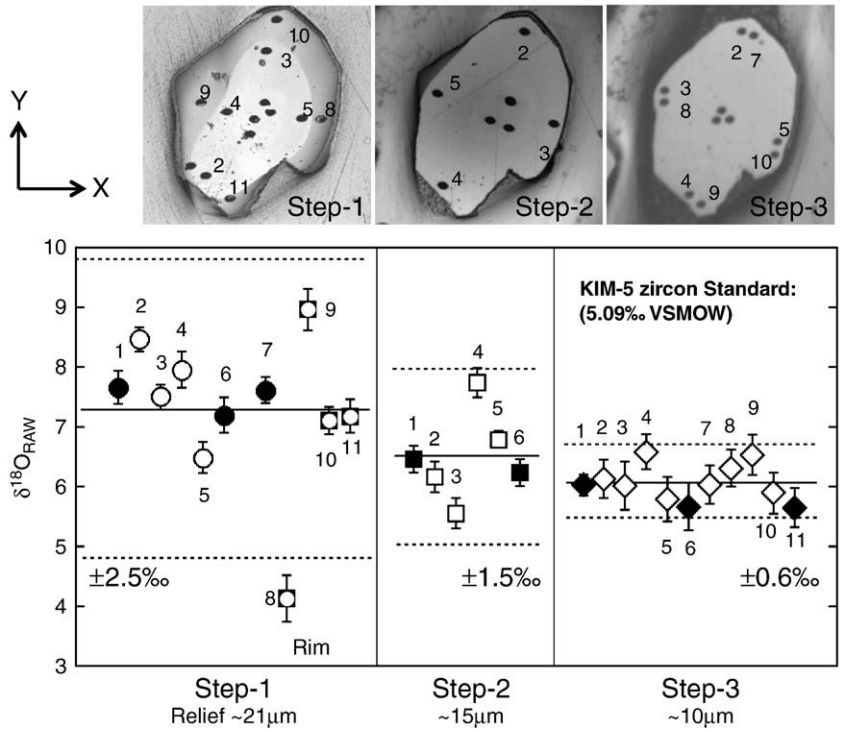

Fig. 10. SIMS oxygen isotope analyses within a single zircon grain showing different levels of polishing relief. Data are shown in Table 2. The rim and center of grain "1" at the center (group 1) of the WI-STD-13 mount (Figs. 6a and 7) were analyzed, showing improvement of reproducibility (2SD) with reduction of relief. Filled symbols are analyses from the center of the grain and open symbols are from the rim. The positions of analysis spots are shown for the rim analyses in the upper images of each test. The solid line and dashed lines in each test represent the average and 2SD of the repeated analyses. The average value cannot be compared directly, because analyses were in different sessions, zircon standard grains with minimal relief were analyzed only during the Step-1, and the uncorrected values of $\delta^{18}O_{RAW}$ of the same standard may change as much as 1‰ in different analytical sessions.

The $\delta^{18}O_{RAW}$ values from near the rim vary as much as 2‰ with an average of 5.19 ± 1.05‰ (2SD, $N = 15$), while the average of the analyses from the center is 5.49 ± 0.26‰ (2SD, $N = 8$). There is a clear trend between the $\delta^{18}O_{RAW}$ values at the rim of the grain and the X–Y coordinates; the $\delta^{18}O_{RAW}$ value decreases with increasing stage X and Y values. This is similar to the results from the rim of a large zircon grain shown in Fig. 10. A 150 μm traverse towards the edge of the grain with increasing stage X values (e.g., data 11, 13, 12, and 10 in Fig. 11) shows progressive depletion of $\delta^{18}O_{RAW}$ values from 5.3‰ to 4.4‰. Data along such a traverse could erroneously be interpreted as a diffusion profile if the effect of polishing relief and variable instrumental bias is not recognized.

3.3. Optimized performance on the rim of diopside standard, 95AK-6

Mount WI-STD-19 contains fragments of the 95AK-6 diopside standard with homogeneous oxygen isotope ratio ($\delta^{18}O = 24.14$‰ VSMOW; "sample 6" in Edwards and Valley, 1998). These grains do not show significant relief (<1 μm). We used a ~10 μm diameter spot to measure $\delta^{18}O_{RAW}$ values within ~20 μm of the edge of one grain and also 100 μm from the edge. As shown in Fig. 12, the average values and the reproducibility of the repeated analyses from the edge and the inside of the grain are indistinguishable; 30.53 ± 0.25‰ (2SD, $N = 7$) and 30.58 ± 0.19‰ (2SD, $N = 6$), respectively. The average value from the edge is only 0.05 ± 0.12‰ (2SE, standard error of the mean) lower than that of inside, indicating that there is no resolvable analytical artifact for measuring the rim of the grains if the polishing relief is minimal.

4. Discussion

4.1. Relationship between sample topography and "X–Y effect"

The tests using samples with variable amounts of polishing relief consistently show large analytical artifacts on $\delta^{18}O_{RAW}$ values that relate to sample topography. The results of multiple grain analyses measuring the center of grains in Fig. 9 show a tendency of improving external precisions with a reduction of polishing relief; from 3‰ (2SD) for 40 μm relief to 0.6‰ (2SD) for 20 μm relief. The result of rim analyses from single grains (KIM-5 zircon and UWQ-1 quartz in Figs. 10 and 11) with relatively smaller polishing relief of 12, 15, 21 μm show external precisions of 1‰, 1.5‰ and 2.5‰ (2SD), respectively. This clearly indicates that the analytical artifact from topography is not solely a function of height of the analyzed positions. In the case of the UWQ-1 quartz grain in Fig. 11, the whole surface is slightly rounded so that the surface of the grain near the rim is always tilted compared to the plane perpendicular to the secondary ion optics. Such a tilted surface would effectively deform the electrostatic field and modify the trajectory of the secondary ions. The degree of inclination seems to increase at the boundary of the grain (such as spots 10, 14, and 19 in Fig. 11c) where we see the largest analytical bias.

A similar artifact could be observed for various other types of polished section that are used for SIMS analyses. Standard polished thin sections are made by gluing rock chips on the surface of the glass slides. If the rock chip is significantly smaller than 25 mm in diameter, the edge of the rock specimen in a standard petrographic thin section should show relief of ~30 μm against the glass surface and this difference may cause analytical artifacts at the periphery of the sample. Likewise, zircon grain mounts prepared for ion microprobe geochronology often show a mirror finished surface, but have a large amount of polishing relief. We typically grind such samples using a 3 μm diamond film to reduce the relief and flatten the surface of the grains before oxygen isotope analyses, which can correlate age and $\delta^{18}O$ in a tiny (≤100 μm) zoned zircon crystals. It should be noted that while controlling relief is clearly important for high precision analysis of $\delta^{18}O$, a clean surface without deep scratches could be more important for some SIMS applications, such as U–Pb dating or trace element analyses where micro-scratches from the coarser grinding

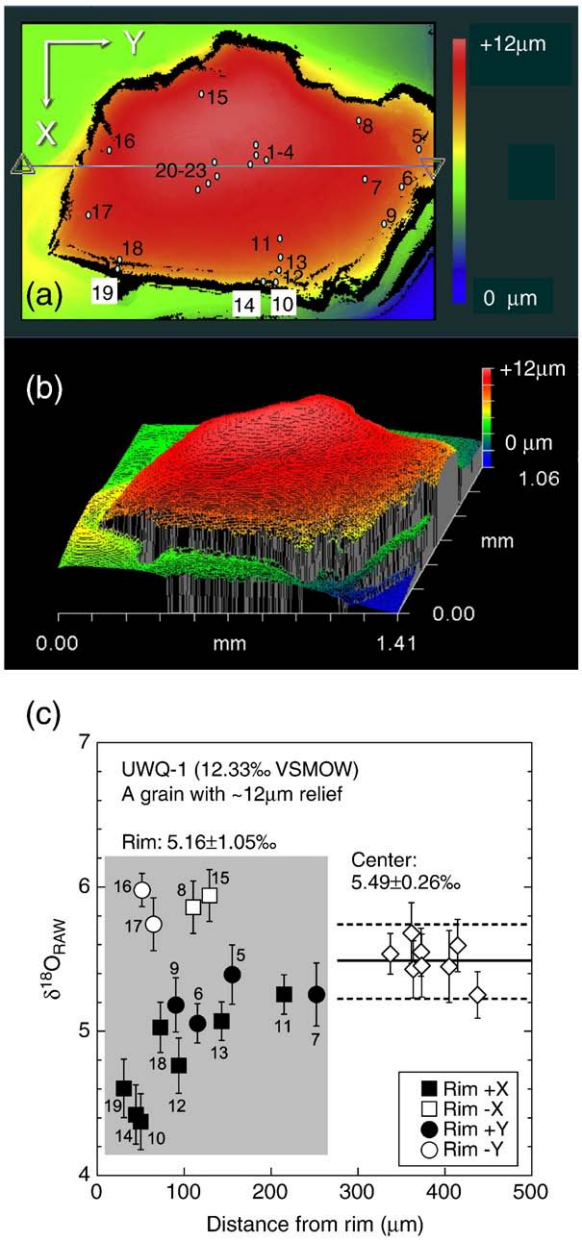

Fig. 11. SIMS oxygen isotope analyses of the center and rim from a quartz standard grain UWQ-1, cast in epoxy with moderate polishing relief (~12 μm). (a, b) Surface topography of a single grain measured using a profilometer. The field of view is 1.4 mm × 1.0 mm. The maximum height difference is 12 μm. The *X* and *Y*-axes of the SIMS analyses are shown as white arrows. Numbers in (a) indicate the sequence of analyses. (c) The $\delta^{18}O_{RAW}$ values from the rim of the grain show false isotope profile. Data are shown as a distance from the rim. The $\delta^{18}O_{RAW}$ values and *XY* coordinates of individual spots are listed in Table A3. Open diamonds are data from the center of the grain (#1-4, and #20-23) that bracket the rim analyses. Open circles, filled circles, open squares and filled squares are data from rim of the grain towards $-Y$, $+Y$, $-X$, and $+X$ directions, respectively. Numbers next to data symbols are same as in (a). The solid line and dashed lines are the average and 2SD of the data from the center of the grain. Most of rim data within 100 μm from the edge of the grain are outside of 2SD defined by the data from the center. Large negative deviations in $\delta^{18}O_{RAW}$ values from those of data at the center are seen from spots located at $+X$ and $+Y$ positions (filled symbols), while data from opposite sides ($-X$ and $-Y$, open symbols) show slightly higher $\delta^{18}O_{RAW}$ values than the center.

steps could result in serious contamination. Therefore, it is important to select the right polishing conditions depending on the purpose of SIMS analyses.

A small X–Y effect is seen from the reproducibility test of the KIM-5 zircon standard if analysis spots are distances of 6–7 mm from the center (shown in Fig. 2) even when the sample is polished with minimal relief. Analyses from pits with negative *X* or *Y* coordinates are slightly higher in $\delta^{18}O_{RAW}$ than the rest of the data (Fig. 2c–d). The effect is small (~0.3‰), but statistically significant, showing the same relationship between *X* and *Y* coordinate and the direction of the shift of $\delta^{18}O_{RAW}$ values. It is very likely that this slight analytical artifact is caused by the topographic effect of the sample holder that covers the outer edge of the polished section at 10 mm from the center of the mount. The sample holder is inserted to the sample stage to which ± 10 kV acceleration voltage is applied. Therefore, the local electrostatic field would be deformed slightly near the edge of the 25 mm section similar to the case of the rim of topographic grains. In the earlier studies, standard grains were sometimes located near the edge of the grain mounts or thin sections for convenience of sample preparation. Likewise, additional standards could be later mounted at the edge of the section because there was no space to drill a hole for "top mounting" at the center. Larger artifacts could be produced if standards are mounted too far from the center and the surface of the section is not completely flat. Slightly convex surfaces are common in cast epoxy mounts and may worsen the topographic effects of the sample holder. As shown in Fig. 2, the maximum artifact normally observed at WiscSIMS is at the level of ~0.3‰ for well polished samples within 6–7 mm of the center. To avoid even these small artifacts, we currently restrict analysis to samples and standards within 5 mm of the center of a mount for highest precision and high accuracy of stable isotope analysis.

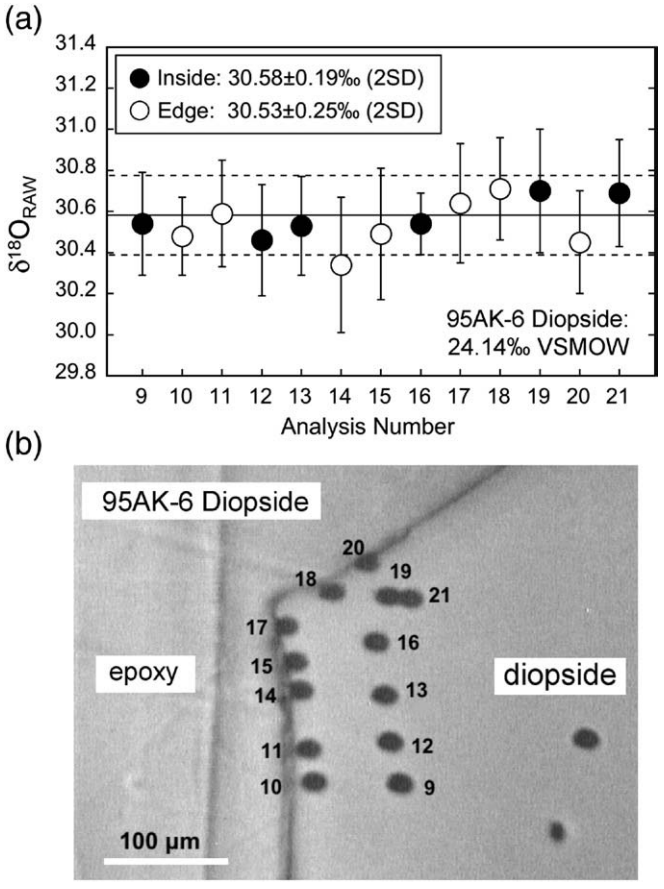

Fig. 12. Optimized SIMS oxygen isotope analyses of the rim of diopside standard (95AK-6) showing minimal polishing relief (<1 μm). (a) The data from edge (open symbols, <20 μm from the edge) and inside (filled symbols, ~100 μm from the edge) are indistinguishable within analytical uncertainty (difference between inside and edge: 0.05 ± 0.12‰, 2SE). (b) Reflected light image of the grain boundary between diopside and epoxy resin. The positions of the SIMS pits are shown with the analysis number; data are in Table A4.

4.2. Published X–Y effects

Large geometric artifacts on the SIMS measured oxygen isotope ratios have been reported recently from various laboratories (Treble et al., 2007; Ickert et al., 2008; Whitehouse and Nemchin, 2009). Ickert et al. (2008), using SHRIMP II, reported significant improvements in the reproducibility of measured values of $\delta^{18}O$ from ±4‰ to ±0.4‰ by the redesigning of the sample mount to have a larger surface area, indicating that the sample geometry induces strong analytical artifacts. Here we discuss two other reports in more detail. These studies use the IMS-1270 and can be compared directly with our results.

Treble et al. (2007) reported that measured oxygen isotope ratios from a standard glass vary as much as 2‰ toward the edge of the mount (within 6 mm from the center). They show that the measured $\delta^{18}O$ values systematically decrease from the center of a 25 mm mount outwards, which is the same tendency observed in this study though their effect is nearly an order of magnitude larger. Whitehouse and Nemchin (2009) reported a series of analytical artifacts on a large lunar zircon grain (0.6–0.8 mm) due to the sample topography and location of the calibrating standards. In their first measurement, the zircon grain was attached to a glass slide by epoxy resin and its polished surface was a few 100 μm above the surface of the glass. The measured data calibrated by zircon standard ($\delta^{18}O = 6.7$‰ VSMOW) are biased by 1‰ higher than the expected value ($\delta^{18}O = 5.5$‰ VSMOW, Nemchin et al., 2006a), leading Nemchin et al. (2006b) to propose an anomalous composition on the Moon. Because of the possibility of a topographic effect, Whitehouse and Nemchin (2009) extracted the zircon grain and remounted it at the center of a new 25 mm epoxy mount with zircon standard (91500) mounted at 5 mm from the sample. The results of these analyses depend on the location of the standard grain; the reported $\delta^{18}O$ values are ~5.7‰ and ~5.1‰ VSMOW when the calibrating standard was located at $Y = -5$ mm and $X = +5$ mm, respectively. If the reported systematic bias is caused by the difference in the instrumental bias of standard at different X–Y coordinates, the measured $\delta^{18}O_{RAW}$ values at $Y = -5$ mm are systematically higher by 0.6‰ than at $X = +5$ mm. As shown in Fig. 2, we observed a similar tendency that the measured $\delta^{18}O_{RAW}$ values at $Y = -6$ mm are higher by 0.4‰ than that at $X = +5.5$ mm. As a final test, Whitehouse and Nemchin (2009) extracted the zircon grain again and remounted so that the standard is located near the center of the mount within 1 mm from the sample, resulting in their final value this lunar zircon to be $\delta^{18}O = 5.7$‰ VSMOW, which is in good agreement with previous analyses of lunar zircons and rocks.

These reported X–Y effects from IMS-1270 instruments described above are generally larger than similar artifacts obtained in this study with a low relief surface (Fig. 2). The magnitude of these published X–Y effects could be due to topography of the particular mount, or it could result from differences in tuning conditions, such as electron gun alignment and secondary ion tuning including selection of slits and aperture sizes. The lack of Z-focusing of the sample stage (in the first measurement of Whitehouse and Nemchin, 2009) would require a large correction of the primary beam positions by secondary ion deflector, which may deform both the electron gun alignment and the secondary ion trajectory. If the secondary ion transmission is significantly lower than 70–90% achieved in this study, the instrumental bias among oxygen isotopes could be more sensitive to small shifts of secondary ion optics due to geometry of the analyzed spots. A small shift of secondary ion trajectory in the entrance slit and field aperture planes will result in the significant instrumental mass fractionation among different isotopes (Schuhmacher et al., 2004), unless the widths of secondary ion beam are significantly narrower than the slit and aperture. The tuning parameters described in this paper (in Table 1) correspond to almost full transmission at the entrance slit plane and at the field aperture plane. Thus, differences in tuning of the secondary beam, reported in our study, help to minimize X–Y effects and may partly explain the differences from tests reported in the literature.

This paper has dealt exclusively with data from "large radius" SIMS instruments because they produce the best accuracy and precision for isotope ratios. Stable isotope ratios can also be measured with smaller SIMS instruments, including the IMS-3f to 7f series and the nanoSIMS, however we are not aware of studies that investigated the analytical artifacts that are described here. It is important to note that inaccuracy due to these artifacts could be significantly worse with other instruments due to differences in ion optics, detection system, or operating protocol.

5. Conclusions

We have developed highly precise and accurate SIMS stable isotope analytical protocols using the IMS-1280 at WiscSIMS. As a result of careful instrumental tuning conditions, stable electronics, improved analysis software, careful standardization, and well-timed analysis protocols, the multicollection FC analyses of $\delta^{18}O$ and $\delta^{17}O$ routinely achieve precision of 0.3‰ (2SD) from a single 10–15 μm spot. The fast analysis time (3–10 min per spot) and long term (>10 h) stability of the magnet and electronics make it possible to obtain more than 150 spot analyses of $\delta^{18}O$ during a 12 h session. Furthermore, precision at the level of ≤1‰ is achieved by using multicollection FC-EM analyses for a primary ion beam sizes of 1–3 μm. Thus, the SIMS is a very useful tool for the high precision and high spatial resolution stable isotope studies that is capable of contributing new observations that could not be obtained before.

X–Y effects are analytical artifacts resulting from the sample topography and location on the sample stage. We found that the effect from well-prepared samples with a flat surface (<1 μm of relief) averages ~0.1‰ and is always less than 0.3‰ in $\delta^{18}O_{RAW}$, which is similar to the analytical uncertainty of a single analysis. In contrast, samples with significant surface topography (>10 μm) show large analytical artifacts as much as 5‰, which highly degrade the accuracy of SIMS analysis. It is found that the average value of $\delta^{18}O_{RAW}$ on high relief samples increased more than 1‰ and that the precision is degraded to ±3‰ compared to those without relief. Therefore, such data are neither accurate nor precise. The magnitude of the X–Y effect on $\delta^{18}O_{RAW}$ correlates with the geometry of the sample and topography from the scale of the relief of a single grain to the shape of the sample holder. These analytical artifacts may be caused by the deformation of local electrostatic field applied on the surface of the sample, which deviates the trajectory of secondary ions of the individual isotopes.

The results from this study clearly indicate that producing a flat sample surface is critical for achieving high precision and high accuracy SIMS stable isotope analyses. The surface profilometer is a useful tool to evaluate the level of topography to test if the sample is suited for the high precision analyses. The present results indicate that for best precision and accuracy, the level of topography should be less than a few μm, and that samples and standards should be mounted together near the center of a sample mount. With proper precautions, the IMS-1280 is capable of significantly improved data quality and smaller analysis spots. Such results are important to many areas of stable isotope geochemistry, especially when samples are very small, precious, or zoned.

Acknowledgements

We thank Brian Hess for sample preparation and Jim Kern for preparing test samples for artificial polishing relief and profilometer analyses. Zeb Page provided unpublished data for estimating the useful yield. We appreciate discussions with Mike Spicuzza, Neal Lord,

and Lee Powell. We also appreciate Paula Peres, Firmino Fernandes, Michel Schumacher and other CAMECA engineers for their support and particularly improvement of the software. Kevin McKeegan and an anonymous reviewer made helpful comments that improved the manuscript. WiscSIMS is partly supported by NSF (EAR03-19230, EAR05-16725, EAR07-44079). This work is supported by NSF (EAR05-09639), DOE (93ER14389, JWV), the NASA Astrobiology Institute, and NASA Cosmochemistry Program (NNX07AI46G, NK).

Appendix A. Supplementary data

Supplementary data associated with this article can be found, in the online version, at doi:10.1016/j.chemgeo.2009.02.012.

References

Baertschi, P., 1976. Absolute ^{18}O content of standard mean ocean water. Earth Planet. Sci. Lett. 31, 341–344.

Bindeman, I.N., Fu, B., Kita, N.T., Valley, J.W., 2008. Origin and evolution of silicic magmatism at Yellowstone based on ion microprobe analysis of isotopically zoned zircons. J. Petrol. 49 (1), 163–193.

Bowman, J.R., Valley, J.W., Kita, N.T., 2009. Mechanisms of oxygen isotopic exchange and isotopic evolution of $^{18}O/^{16}O$-depleted periclase zone marbles in the Alta aureole, Utah – insights from ion microprobe analysis of calcite. Contrib. Min. Pet., 157, 77–93.

Cavosie, A.J., Valley, J.W., Wilde, S.A., E.I.M.F., 2005. Magmatic $\delta^{18}O$ in 4400–3900 Ma detrital zircons: a record of the alteration and recycling of crust in the Early Archean. Earth Planet. Sci. Lett. 235 (3–4), 663–681.

Clayton, R.N., Mayeda, T.K., Goswami, J.N., Olsen, E.J., 1991. Oxygen isotope studies of ordinary chondrites. Geochim. Cosmochim. Acta, 55 (8), 2317–2337.

Desbois, G., Ingrin, J., Kita, N.T., Valley, J.W., Deloule, E., 2007. New constraints on metamorphic history of Adirondack diopsides (New York, U.S.A.): Al and $\delta^{18}O$ profiles. Am. Min. 92, 453–459.

Downes, H., Mittlefehldt, D.W., Kita, N.T., Valley, J.W., 2008. Evidence from polymict ureilite meteorites for a disrupted and re-accreted single ureilite parent asteroid gardened by several distinct impactors. Geochim. Cosmochim. Acta 72, 4825–4844.

Edwards, K.J., Valley, J.W., 1998. Oxygen isotope diffusion and zoning in diopside: the importance of water fugacity during cooling. Geochim. Cosmochim. Acta 62 (13), 2265–2277.

Eiler, J.M., Graham, C., Valley, J.W., 1997a. SIMS analysis of oxygen isotopes: matrix effects in complex minerals and glasses. Chem. Geol. 138, 221–244.

Eiler, J.M., Valley, J.W., Graham, C.M., 1997b. Oxygen and carbon isotope analysis by SIMS:A case study of the Martian Meteorite ALH84001. In: Gillen, G., Larean, R., Bennett, J., Stevie, F. (Eds.), SIMS XI Meeting. Wiley, NY, pp. 47–50.

Eiler, J.M., Schiano, P., Valley, J.W., Kita, N.T., Stolper, E.M., 2007. Oxygen-isotope and trace element constraints on the origins of silica-rich melts in the subarc mantle. Geochem. Geophys. Geosyst. 8, Q09012.

Gurenko, A.A., Chaussidon, M., Schmincke, H.U., 2001. Magma ascent and contamination beneath one intraplate volcano; evidence from S and O isotopes in glass inclusions and their host clinopyroxenes from Miocene basaltic hyaloclastites southwest of Gran Canaria (Canary Islands). Geochim. Cosmochim. Acta 65, 4359–4374.

Hervig, R.L., Williams, P., Thomas, R.M., Schauers, S.N., Steele, I.M., 1992. Microanalysis of oxygen isotopes in insulators by secondary ion mass-spectrometry. Int. J. Mass Spectrom. Ion Process. 120, 45–63.

Ickert, R.B., Hiess, J., Williams, I.S., Holden, P., Ireland, T.R., Lanc, P., Schram, N., Foster, J.J., Clement, S.W., 2008. Determining high precision, in situ, oxygen isotope ratios with a SHRIMP II: analyses of MPI-DING silicate-glass reference materials and zircon from contrasting granites. Chem. Geol. 257, 114–128.

Ireland, T.R., 1995. Ion microprobe mass spectrometry: techniques and applications in cosmochemistry, geochemistry, and geochronology. In: Hyman, M., Rowe, M. (Eds.), Advances in Analytical Geochemistry, vol. 2, pp. 1–118.

Kelly, J.L., Fu, B., Kita, N.T., Valley, J.W., 2007. Optically continuous silcrete quartz cements of the St. Peter Sandstone: high precision oxygen isotope analysis by ion microprobe. Geochim. Cosmochim. Acta 71, 3812–3832.

Kita, N.T., Ikeda, Y., Togashi, S., Liu, Y.Z., Morishita, Y., Weisberg, M.K., 2004. Origin of ureilites inferred from a SIMS oxygen isotopic and trace element study of clasts in the Dar al Gani 319 polymict ureilite. Geochim. Cosmochim. Acta. 68, 4213–4235.

Kita, N.T., Ushikubo, T., Fu, B., Spicuzza, M.J., Valley, J.W., 2007. Analytical developments on oxygen three isotope analyses using a new generation ion microprobe IMS-1280. Lunar Planet. Sci. Conf., vol. 38. abstr. #1981.

Kita, N.T., Kimura, M., Ushikubo, T., Valley, J.W., 2008. Oxygen isotope systematics of chondrules from the least equilibrated H chondrite. Lunar Planet. Sci. Conf., vol. 39. Abstr. #2059.

Knight, K.B., Kita, N.T., Mendybaev, R.A., Richter, F.M., Davis, A.M., Valley, J.W., in press. Si isotope fractionation of CAI-like vacuum evaporation residues. Geochim. Cosmochim. Acta.

Kozdon, R., Ushikubo, T., Kita, N.T., Valley, J.W., 2009. Intratest oxygen isotope variability in the planktonic foraminifer N. pachyderma: Real vs. apparent vital effects by ion microprobe. Chem. Geol., 258, 327–337.

Lancaster, P.J., Fu, B., Page, F.Z., Kita, N.T., Bickford, M.E., Hill, B.M., McLelland, J.M., Valley, J.W., 2009. Genesis of metapelitic migmatites in the Adirondack Mts., New York. J. Meta. Geol. 27, 41–54.

Leshin, L.A., Rubin, A.E., McKeegan, K.D., 1997. The oxygen isotopic composition of olivine and pyroxene from CI chondrites. Geochim. Cosmochim. Acta 61, 835–845.

Liu, Y., Taylor, L.A., Sarbadhikari, A.B., Valley, J.W., Ushikubo, T., Spicuzza, M.K., Kita, N., Stepanov, A., Shatsky, V., Sobolev, N.V., 2008. Diamond genesis in the world's largest diamondiferous eclogite, Part II: in-situ isotope study of diamond and mineral inclusions. 9th International Kimberlite Conference Extended. Abstract No. 9IKC-A-00188.

McKeegan, K.D., 1987. Oxygen isotopes in refractory stratospheric dust particles: proof of extraterrestrial origin. Science 237, 1468–1471.

McKeegan, K.D., Leshin, L.A., Russell, S.S., MacPherson, G.J., 1998. Oxygen isotopic abundances in calcium-aluminum-rich inclusions from ordinary chondrites: implications for nebular heterogeneity. Science 280, 414–418.

Moser, D.E., Bowman, J.R., Wooden, J., Valley, J.W., Mazdab, F., Kita, N., 2008. Creation of a continent recorded in zircon zoning. Geology 36, 239–242.

Nakamura, T., Noguchi, T., Tsuchiyama, A., Ushikubo, T., Kita, N.T., Valley, J.W., Zolensky, M.E., Kakazu, Y., Sakamoto, K., Mashio, E., Uesugi, K., Nakano, T., 2008. Chondrule-like objects in short-period comet 81P/Wild 2. Science 321, 1664–1667.

Nemchin, A.A., Whitehouse, M.J., Pidgeon, R.T., Meyer, C., 2006a. Oxygen isotopic signature of 4.4–3.9 Ga zircons as a monitor of differentiation processes on the Moon. Geochim. Cosmochim. Acta 70, 1864–1872.

Nemchin, A.A., Whitehouse, M.J., Pidgeon, R.T., Meyer, C., 2006b. Heavy isotope composition of oxygen in zircon from soil sample 14163: lunar perspective of an early ocean on the earth. Lunar Planet. Sci. Conf., vol. 37. Abstr. #1593.

Orland, I.J., Bar-Matthews, M., Kita, N.T., Ayalon, A., Matthews, A., Valley, J.W., 2009. Climate deterioration in the eastern Mediterranean from 200 BC to 1100 AD as revealed by ion microprobe analysis of speleothems from Soreq Cave, Israel. Quat. Res., 71, 27–35.

O'Neil, J.R., 1986. Terminology and standards. In: Valley, J.W., Taylor, H.P., O'Neil, J.R. (Eds.), Stable Isotopes in High Temperature Geological Processes. Min. Soc. Am. Rev. in Mineral., vol. 16, pp. 561–570.

Page, F.Z., Ushikubo, T., Kita, N.T., Riciputi, L.R., Valley, J.W., 2007. High-precision oxygen isotope analysis of picogram samples reveals 2 μm gradients and slow diffusion in zircon. Amer. Min. 92, 1772–1775.

Riciputi, L.R., Paterson, B.A., Ripperdan, R.L., 1998. Measurement of light stable isotope ratios by SIMS: matrix effects for oxygen, carbon, and sulfur isotopes in minerals. Int. J. Mass Spectrom. 178 (1–2), 81–112.

Rusk, B., Hofstra, A., Leach, D., Lowers, H., Koenig, A., Kita, N.T., Valley, J.W., 2007. Combined cathodoluminescence, oxygen isotopes, and trace element study of vein quartz from several hydrothermal ore deposits. GSA Abstr. Prog. 39, 396.

Shimizu, N., Semet, M.P., Allègre, C.J., 1978. Geochemical applications of quantitative ionmicroprobe analysis. Geochim. Cosmochim. Acta 42, 1321–1334.

Schuhmacher, M., Fernandes, F., De Chambost, E., 2004. Achieving high reproducibility isotope ratios with the Cameca IMS1270 in the multicollection mode. Appl. Surf. Sci. 231–232, 878–882.

Treble, P.C., Chappell, J., Gagan, M.K., McKeegan, K.D., Harrison, T.M., 2005. In situ measurement of seasonal delta O-18 variations and analysis of isotopic trends in a modem speleothem from southwest Australia. Earth Planet. Sci. Lett. 233 (1–2), 17–32.

Treble, P.C., Schmitt, A.K., Edwards, R.L., McKeegan, K.D., Harrison, T.M., Grove, M., Cheng, H., Wang, Y.J., 2007. High resolution Secondary Ionisation Mass Spectrometry (SIMS) delta O-18 analyses of Hulu Cave speleothem at the time of Heinrich Event 1. Chem. Geol. 238 (3–4), 197–212.

Ushikubo, T., Kita, N.T., Cavosie, A.J., Wilde, S.A., Rudnick, R.L., Valley, J.W., 2008. Lithium in Jack Hills zircons: recycling of Earth's earliest crust. Earth Planet. Sci. Lett. 272, 666–676.

Valley, J.W., 2003. Oxygen isotopes in zircon. In: Hanchar, J.M., Hoskin, P.W.O. (Eds.), Zircon. Rev. Mineral. Geochem., vol. 53, pp. 343–385.

Valley, J.W., Graham, C.M., 1991. Ion microprobe analysis of oxygen isotope ratios in metamorphic magnetite-diffusion reequilibration and implications for thermal history. Contr. Mineral. Petrol. 109, 38–52.

Valley, J.W., Kitchen, N.E., Kohn, M.J., Niendorf, C.R., Spicuzza, M.J., 1995. UWG-2, A garnet standard for oxygen isotope ratio: strategies for high precision and accuracy with laser heating. Geochim. Cosmochim. Acta 59, 5223–5231.

Valley, J.W., Graham, C.M., Harte, B., Kinny, P., Eiler, J.M., 1998. Ion microprobe analysis of oxygen, carbon, and hydrogen isotope ratios. In: McKibben, M.A., et al. (Ed.), Soc. Econ. Geol. Rev. in Econ. Geol., vol. 7, pp. 73–98.

Vielzeuf, D., Champenois, M., Valley, J.W., Brunet, F., Devidal, J.L., 2005. SIMS analysis of oxygen isotopes: matrix effects in Fe–Mg–Ca garnets. Chem. Geol. 223, 208–226.

Yurimoto, H., Ito, M., Nagasawa, H., 1998. Oxygen isotope exchange between refractory inclusion in Allende and solar nebula gas. Science 282, 1874–1877.

Weidel, B.C., Ushikubo, T., Carpenter, S.R., Kita, N.T., Cole, J.J., Kitchell, J.F., Pace, M.L., Valley, J.W., 2007. Diary of a bluegill (Lempomis macrochirus): daily $\delta^{13}C$ and $\delta^{18}O$ records in otoliths by ion microprobe. Can. J. Fish. Aquat. Sci. 64, 1641–1645.

Whitehouse, M.J., Nemchin, A.A., Nagasawa, H., 2009. High precision, high accuracy measurement of oxygen isotopes in a large lunar zircon by SIMS. Chemi. Geol. 261, 31–41.

Wilde, S.A., Valley, J.W., Kita, N.T., Cavosie, A.J., Liu, D.Y., 2008. SHRIMP U–Pb and CAMECA 1280 oxygen isotope results from ancient detrital zircons in the Caozhuang quartzite, Eastern Hebei, North China Craton: Evidence for crustal reworking 3.8 Ga ago. Am. J. Sci. 308 (3), 185–199.